LAWRENCE
LIVERMORE
NATIONAL
LABORATORY

LLNL-TR-424425

Atmospheric Stability Impacts on Power Curves of Tall Wind Turbines - An Analysis of a West Coast North American Wind Farm

S. Wharton, J. K. Lundquist

February 23, 2010

Disclaimer

This work performed under the auspices of the U.S. Department of Energy by Lawrence Livermore National Laboratory under Contract DE-AC52-07NA27344.

Atmospheric Stability Impacts on Power Curves of Tall Wind Turbines – An Analysis of a West Coast North American Wind Farm

Sonia Wharton[1] and Julie K. Lundquist[1,2]

[1]Atmospheric, Earth and Energy Division, Lawrence Livermore National Lab, P.O. Box 808, L-103, Livermore, CA 94551,

[2]Department of Atmospheric and Ocean Sciences, University of Colorado at Boulder, CUB-311, Boulder, CO 80309-0311

LLNL-TR-424425

Abstract

Tall wind turbines, with hub heights at 80 m or above, can extract large amounts of energy from the atmosphere because they are likely to encounter higher wind speeds, but they face challenges given the complex nature of wind flow and turbulence at these heights in the boundary layer. Depending on whether the boundary layer is stable, neutral, or convective, the mean wind speed, direction, and turbulence properties may vary greatly across the tall turbine swept area (40 to 120 m AGL). This variability can cause tall turbines to produce difference amounts of power during time periods with identical hub height wind speeds. Using meteorological and power generation data from a West Coast North American wind farm over a one-year period, our study synthesizes standard wind park observations, such as wind speed from turbine nacelles and sparse meteorological tower observations, with high-resolution profiles of wind speed and turbulence from a remote sensing platform, to quantify the impact of atmospheric stability on power output. We first compare approaches to defining atmospheric stability. The standard, limited, wind farm operations enable the calculation only of a wind shear exponent (α) or turbulence intensity (I_U) from cup anemometers, while the presence at this wind farm of a SODAR enables the direct observation of turbulent kinetic energy (*TKE*) throughout the turbine rotor disk. Additionally, a nearby research meteorological station provided observations of the Obukhov length, *L,* a direct measure of atmospheric stability. In general, the stability parameters α, I_U, and *TKE* are in high agreement with the more physically-robust *L,* with *TKE* exhibiting the best agreement with *L*. Using these metrics, data periods are segregated by stability class to investigate power performance dependencies. Power output at this wind farm is highly correlated with atmospheric stability during the spring and summer months, while atmospheric stability exerts little impact on power output during the winter and autumn periods.

During the spring and summer seasons, power output for a given wind speed was significantly higher during stable conditions and significantly lower during strongly convective conditions: power output differences approached 20% between stable and convective regimes. The dependency of stability on power output was apparent only when both turbulence and the shape of the wind speed profile were considered. Turbulence is one of the mechanisms by which atmospheric stability affects a turbine's power curve at this particular site, and measurements of turbulence can yield actionable insights into wind turbine behavior.

Table of Contents

Abstract **2**

1. Introduction **5**

2. Previous studies **9**

3. Methods **12**

3.1 Overview of site and available data 12

3.2 Meteorological measurements and stability parameters 14

3.3 Stability classifications 19

3.4 Equivalent wind speed 21

3.5 Comparison of available wind speeds 23

3.6 Evaluation of power performance 24

4. Results **26**

4.1 Seasonal wind speed and direction at the site 26

4.2 Stability parameter analysis and comparison 28

4.3 Stability influence on wind velocity and turbulence profiles 35

4.4 Seasonal power output at an individual turbine 40

4.5 Wind speed representation in power curves 42

4.6 Stability parameter influence on power performance 43

4.6.1 *nacelle* I_U 44

4.6.2 *SODAR* α 47

4.6.3 *SODAR* I_U 49

4.6.4 *SODAR TKE* 52

4.6.5 Summary of power dependency on stability regime 54

5. Discussion **57**

6. Conclusions **62**

7. References **64**

List of Tables **69**

List of Figures **70**

1. Introduction

As utility-scale deployment of wind energy expands, turbine sizes and generating capacities also increase. For example, the wind energy industry in the United States brought over 5,000 turbines online in 2008, with an average capacity of 1.67 MW (AWEA 2009). Over half of the turbines installed in 2008 were 1.5 MW in capacity, with hub heights ranging from 60 m to 100 m above the surface and rotor diameters on the order of 80 m. Turbines with larger capacities generally utilize higher hub heights: the Enercon E-126 6 MW turbine is designed for a hub height of 135 m, with a rotor disk extending to 198 m (Enercon 2009). As turbines penetrate higher altitudes, the area swept by the blades expands beyond the atmospheric surface layer and into regions with complex flows driven by shear stratification or turbulent mixing (Larsen et al. 2007). While wind velocities in the turbine rotor (i.e., the swept area) largely determine the amount of power that is generated, wind shear and turbulence intensity also appear to play a role in power output (e.g., Elliott and Cadogan 1990, Motta et al. 2005, Sumner and Masson 2006, Gottschall and Peinke 2008, van den Berg 2008).

In an averaged sense, wind velocity typically increases logarithmically with height from a minimum found just above the ground surface to a maximum near the top of the boundary layer, although the shape of the profile changes with atmospheric stability. Wind velocity also varies across seasonal, synoptic, diurnal, and higher frequency (i.e., turbulence) time scales. Wind farms over land generally experience strong diurnal effects with large differences between daytime and nighttime wind speeds. Generally at night, turbulent motions are subdued, the boundary layer is statically stable, and air flow becomes stratified at heights encountered by the wind turbine. This stratification can lead to high shear conditions in the rotor blade swept-area

with wind maxima, or low-level jets, between 100 and 300 m above the surface, near the top of modern turbine rotors. During the day, turbulent motions are enhanced, the boundary layer is well mixed or unstable, and wind shear is very low so that wind speeds at the top of the rotor are similar to those at the lower blade tip.

Accurate descriptions of how wind velocity and turbulence vary across the rotor may be possible through characterization of the stability of the lower boundary layer. Atmospheric stability is largely driven by thermal gradients (static stability), and by frictional drag along the ground surface and wind shear aloft (dynamic stability). Unstable atmospheric conditions usually occur during daylight hours when surface heating causes air to rise, resulting in large-scale turbulent eddies and turbulent mixing which reduces vertical gradients of temperature and velocity. If the rising air parcels are in thermal equilibrium with the surrounding air, the boundary layer is said to be neutrally stable. Neutral conditions often occur when wind speeds are very high and vertical gradients are constant or during dawn and dusk when stability conditions in the boundary layer transition. Stable conditions occur when vertical motion is suppressed (negative buoyancy) and turbulence is dominated either by mechanical forces near the surface (e.g. friction with the ground surface) or high wind shear aloft (e.g. nocturnal low-level jet). A stable boundary layer is characterized by very little vertical mixing and strong gradients of temperature and velocity.

Stability classification schemes for the lower boundary layer have previously been based on vertical profiles of virtual potential temperature θ_v (i.e., the lapse rate $\frac{d\theta}{dz}$), the gradient Richardson number Ri (e.g., Kaimal and Finnigan 1994, Magnusson and Smedman 1999) and the surface-layer Obukhov length L (e.g. Mahrt et al. 1998, Mahrt 1999). The lapse rate gives

the most straightforward indication of whether the boundary layer is statically stable (subadiabatic lapse rate), statically unstable (superadiabatic lapse rate) or neutral (adiabatic lapse) although a temperature profile requires either multiple instruments on a very tall meteorological tower or a remote sensing platform. Because of these logistical constraints, boundary-layer studies often rely on the surface-based Obukhov length to characterize stability, which requires a single heat flux measurement near the ground. This surface-based approach may not be ideal in wind power applications because L does not account for top-down forced boundary layers such as those that occur during low-level jets (Mahrt et al. 2002).

Wind farms have conventionally inferred local stability conditions from either a measure of wind shear, estimated from two to four wind speed measurement heights, or turbulence intensity, often from a single height cup anemometer. High magnitudes of wind shear suggest a stable boundary layer and the turbine blades are likely to encounter strongly stratified flow (e.g., much higher wind speeds at the top of the rotor than at the bottom) across the swept-area. Low values of wind shear indicate convective or well-mixed conditions across the rotor and a more uniform velocity profile. The second convention for estimating stability is based on the relative amount of turbulence present in the atmosphere, or turbulence intensity. A stable atmosphere is generally characterized by having very low amounts of turbulence while a convective atmosphere will be more turbulent. High amounts of turbulence can put significant aerodynamic loads on the turbine and cause fatigue damage to the turbine rotor (Kelley et al. 2001, Hand et al. 2003).

The site presented here is unique from other wind farms in regard to: (1) the presence of both marine and terrestrial boundary layers over mildly complex terrain, (2) local orographic relief creates channeled flow leading to a dominate wind direction at all heights within the rotor

swept-area (i.e., very little directional shear), (3) several seasons of turbine and meteorological data were available, and (4) a robust network of instrumentation was available which allowed for the comparison of the swept-area wind profile to hub-height measurements of wind velocity, turbulence intensity, and power at the individual turbines. In particular, this site employed remote sensing instrumentation, a SODAR, to measure wind profiles throughout the blade-swept area. As such, this robust dataset enables quantification of the dependence of wind power collection efficiency with atmospheric stability conditions and answers the question: How does atmospheric stability impact a tall turbine's power curve?

This report is divided into four parts. A review of previous investigations into the effects of atmospheric stability and turbulence intensity on wind turbine power production appears in Section 2. Section 3 provides background information on the wind farm and the meteorology experienced during the study year, as well as the methods used to quantify atmospheric stability, wind shear, turbulence intensity, and power collection at the turbines at this wind farm. Section 4 presents the results of the investigation, including a detailed analysis of the impacts of boundary layer stability on power collection at an individual turbine. A final discussion of the work presented here is given in Section 5.

2. Previous Studies

Previous investigations of the accuracy of turbine power curves have noted a dependency of power performance on wind shear and turbulence intensity, although very few of these studies use observations of power performance data from three-bladed turbines with hub heights above 60 m. These investigations include early studies by Christensen and Dragt (1986), Fransden (1987), Elliott and Cadogan (1990), and Rohatogi (1996), as well as more recent research by van den Berg (2008), Tindal et al. (2008), Antoniou et al. (2009a), Rareshide et al. (2009), and Wagner et al. (2009). Some stability studies have focused on specific atmospheric phenomena found in the lower boundary layer, including the nocturnal low-level jet (LLJ) which produces a wind maxima (Blackadar 1957, Stull 1988, Banta 2008) at heights near the top of the turbine rotor (e.g., Kelley et al. 2004, Emeis et al. 2007, Cosack et al. 2007, Pichugina et al. 2008, Storm et al. 2009). Other teams have focused on the sensitivity of power curves to wind shear (Hunter et al. 2001, Rareshide et al. 2009, Wagner et al. 2009) and turbulence intensity (Elliott and Cadogan 1990, Kaiser et al. 2003, Honhoff 2007, Tindal et al. 2008, Rareshide et al. 2009).

Wind shear is often estimated in the rotor disk by the wind shear exponent, α, where α equal to zero represents a perfectly well-mixed profile with no shear across the rotor disk and α equal to 0.3 represents a highly stratified profile with large shear across the rotor disk. A number of studies have shown that wind shear has an effect on power output although the results are not universal. Rareshide et al. (2009) found that moderate to high wind shear conditions (α >0.2) at moderate wind speeds (7.5 to 8.5 m s^{-1}) led to higher power output at a U.S. Great Plains wind farm than when wind shear was low. In contrast, Wagner et al. (2009) observed that very high wind shear (α > 0.35) decreased power output by 42% as compared to no shear conditions in a modeling study based on 90 m tall Siemens 3.6 MW turbines. A third study done

by Hunter et al. (2001) found that high wind shear at an English wind farm had different effects on power output depending on the average hub-height wind speed. At moderate wind speeds (~ 5.5 m s^{-1}), 20% more power was generated as wind shear approached 0.3 than when wind shear was zero. For wind speeds above 8.5 m s^{-1}, high magnitudes of wind shear had the opposite effect on power output. At this velocity, higher values of wind shear actually led to lower power output from the turbines. (The type and hub heights of turbines are unidentified in Hunter et al. 2001 and Rareshide et al. 2009).

Because large wind shear can either positively or negatively impact power generation, another mechanism, turbulence intensity, likely exerts an influence on power generation. Elliott and Cadogan (1990), in one of the earliest and most notable studies, suggest that separate power curves for different turbulent regimes should be calculated to distinguish the effects of turbulence intensity on power production. At a West Coast site with two-bladed MOD-2 2.5 MW turbines (60 m hub heights), differences in power generation approached 300 to 400 kW between high turbulence (more power) and low turbulence (less power) conditions during moderate to high wind speeds. Further analysis showed that at low turbulence intensities, hub-height wind speed overestimated the rotor-averaged velocity by as much as 1 m s^{-1} or more because wind shear in the upper half of the rotor was either negative or near zero. At high turbulence intensities, they observed little or no difference between hub-height wind speed and rotor-averaged wind speed. This distinction led to more power being extracted from the wind during times of high turbulence because wind speeds in the upper half of the rotor were actually greater than during times of low turbulence. Although these turbines approach the hub heights of many of the modern industrial-scale turbines, the behavior of these two-bladed turbines may differ from the three-bladed turbines found in broad use today.

The effect of both shear and turbulence on wind turbine power performance was examined by Wagner et al. (2009) whereby they used actual atmospheric profiles in a model simulation of tall turbine performance. They found that by incorporating both turbulence and wind shear into an "equivalent" or rotor-averaged wind speed, they were able to obtain more accurate power curves than by using hub-height wind speed alone. Despite studies such as this one which suggests that wind shear and turbulence impact power production, power curves are still typically made as a function of hub-height wind speed, without information on wind velocity and turbulence intensity across the entire rotor disk. This approach is continued primarily because of the challenge of fielding meteorological towers or remote sensing platforms to provide observations at multiple heights spanning the rotor disk. By plotting power as a function of hub-height wind speed, the effects of wind shear and turbulence intensity described above may be hidden, and a turbine can be seen to perform sub-optimally. In the present study, using a high resolution SODAR which can provide measurements of wind velocity and atmospheric turbulence throughout the rotor disk, we explore these impacts of shear and turbulence at a farm with modern three-bladed turbines at hub heights of 80 m through multiple seasons, using meteorological and turbine performance observations.

3. Methods

3.1 Overview of site and available data

The data in this study were collected at a wind farm located in western North America at an elevation of near-sea level with some marine boundary layer influences. The area experiences strong land/sea temperature gradients, particularly during the summer months when the land is much warmer than the coastal Pacific waters; this gradient produces winds consistently from the westerly or southwesterly direction. This site has two distinct seasons: a wet, cool winter and dry, warm summer with very little convective storm activity occurring during the warm season. The landscape is grassland and rolling hills of mildly complex terrain and elevation variations less than 100 m. Portions of the site are used as grazing land.

A number of horizontal-axis, three-bladed wind turbines with a rotor diameter of nominally 80 m are in operation at the wind farm. The blades interact with the instantaneous wind speed, $u(t)$, within a disk-shaped area across heights of 40 m to 120 m above the ground level (AGL), where 40 m is the minimum blade tip height and 120 m is the maximum blade tip height. The nacelle and power generator are located at 80 m AGL (referred to as hub-height). Cup anemometers are sited on the end of nacelle hubs, providing hub-height estimates of wind speed and turbulence intensity as discussed below. A subset of six turbines from the site is selected for analysis in this study; these turbines are all upwind of other turbines and other obstacles.

The wind farm employs two meteorological towers with vertical arrays of cup anemometers from 30 m to 80 m AGL (hub-height). Additionally, a SODAR collects high resolution, three-axis wind velocity data during most of the year-long study period. High resolution SODAR data enables the calculation of a wind shear exponent, α, horizontal

turbulence intensity, I_U, and turbulent kinetic energy (*TKE)* at all heights within the rotor disk as discussed in detail below. In addition, the Obukhov length, L is obtained from three-axis wind velocity and surface heat flux measurements from an off-site research station approximately 10 km away in similar terrain. All measurements (meteorological tower wind speed, SODAR wind speed and direction, and nacelle wind speed and power output) except for the Obukhov length are averaged over a 10-minute time period. Measurements of wind speed and temperature used in the Obukhov length calculation are available as 30-minute averages. Full instrumentation details are listed in Table 1.

	Instrument	Time resolution	Location	Measurement height (m)	Data collected	# of site locations
wind speed	NRG cup anemometer	10 min	turbine nacelle	80	U, σ_U	6
	NRG cup anemometer	10 min	on-site 50-m tower	30, 40, 50	U, σ_U	1
	NRG cup anemometer	10 min	on-site 80-m tower	50, 60, 80	U, σ_U	1
	SODAR	10 min	on-site	20,30,40,50,60,70, 80,90,100,110,120, 130,140,150,160, 170,180,190,200	u, v, w, σ_u, σ_v, σ_w	3 (one roving system)
	3-D sonic anemometer	30 min	off-site tower	3	u(t), v(t),w(t), u, v, w, u', v', w'	1
wind direction	wind vane	10 min	turbine nacelle	80	degree	6
	wind vane	10 min	on-site 50-m tower	47	degree	1, not fully operational
	wind vane	10 min	on-site 80-m tower	77	degree	1, not fully operational
	SODAR	10 min	on-site	20,30,40,50,60,70, 80,90,100,110,120, 130,140,150,160, 170,180,190,200	degree	3 (one roving system)
	3-D sonic anemometer	30 min	off-site tower	3	degree	1
air temperature	temperature sensor	10 min	on-site 50-m tower	47	°C	1, not fully operational
	temperature sensor	10 min	on-site 80-m tower	77	°C	1, not fully operational
	3-D sonic anemometer, relative humidity/ temperature sensor	30 min	off-site meteorological tower	3	θ_v, °C	1

Table 1: List of available meteorological instrumentation, variables measured, and measurement heights.

Throughout this paper we define the wind velocities as the following: u is mean wind speed in the streamwise direction, v is mean wind speed in the crosswind direction, w is mean wind speed in the vertical direction, and u', v', and w' are deviations of the instantaneous wind speed components ($u(t)$, $v(t)$, and $w(t)$) from the mean wind speed (u, v, and w), such that, $u' = u(t) - u$. The total horizontal mean wind speed, U, is the vector sum of the two horizontal velocities, where, $U = \sqrt{u^2 + v^2}$. All analyses were done using the statistical software package ORIGIN 8 (OriginLab Corp., Northampton, MA, USA). We report the Pearson's correlation coefficient (r) and one-way ANOVA P-value (P) at a significance level equal to the 95th confidence level ($P < 0.05$).

3.2 Meteorological measurements and stability parameters

Vertical profiles of mean wind speed are available at two meteorological towers (50 m and 80 m tall) for this study. Three cup anemometers (NRG IceFree, NRG Systems, Hinesburg, Vermont) are mounted on the 50 m tall tower at heights of 30 m, 40 m, and 50 m AGL. The 80 m tall tower was equipped with three cup anemometers at heights equal to 50 m, 60 m, and 80 m AGL. The 80 m tall tower also had measurements of the standard deviation of mean wind speed at each of the three heights. The cup anemometers measure the mean horizontal wind velocity (U, m s^{-1}) at a sampling rate of 1 Hz with an accuracy of 0.3 m s^{-1}. Wind direction and air temperature are measured at a single height on each tower: 47 m and 77 m. Frequent data outages in air temperature measurements, as well as the horizontal distance between the two meteorological towers, make it impossible to use the vertical temperature profiles to determine atmospheric stability at this site.

SODAR measurements of three components of wind speed (m s^{-1}) and wind direction are also available during much of the study period. SODAR emits high frequency acoustic signals in three (*u*, *v*, and *w*) directions and calculates wind speed by analyzing the frequency shift in spectral energy in the return signal (Coulter and Kallistrova 1999, Crescenti 1997). The wind vectors are measured at 10 m height intervals from 20 m to 200 m, for a total of 19 height levels above the ground surface using a 4500 Hz Doppler Sound Detection and Ranging (SODAR) (Model4000, Atmospheric Systems Corporation, Santa Clarita, CA) at a sampling rate of 0.4 Hz. The SODAR operated from July 2007 to May 2008 with major outages in the rainy season (November, December and January). On average, daytime (nighttime) data recovery was greater than 95% (90%) at the 40 m height, 90% (85%) at 80 m, and 75% (83%) at 120 m AGL. The instrument was not stationary during the study period and was moved to three site locations within the wind farm, corresponding to the periods: July 2007 to mid-August 2007, mid-August 2007 to September 2007, and October 2007 to May 2008.

SODAR and cup anemometer wind velocities were used to calculate the dimensionless wind shear exponent, α, using a power law expression (Eq 1) (Elliott et al. 1987),

$$U(z) = U_R(\frac{z}{z_R})^{\alpha} \quad (1)$$

where U is the mean horizontal wind speed (m s^{-1}) at height z (m), and U_R is the mean horizontal wind speed (m s^{-1}) at reference height z_R (m). In Equation (1) the reference height (z_R) is by convention closer to the ground than height z. We calculated four distinct α parameters. Three α-values were calculated using SODAR: α_{40_120} estimates wind shear across the entire swept area of the rotor, α_{40_80} estimates wind shear across the lower half of the swept area, and α_{80_120}

estimates wind shear across the upper half of the swept area. A fourth α-value, $\alpha_{50\_80,}$ was calculated using the meteorological tower cup anemometers at heights of 80 m and 50 m for comparison to the SODAR shear exponent α_{40_80}. A constant α-value of 1/7 (0.144) is commonly used to extrapolate the wind speed taken at a reference height (often near the surface) to all other heights within the blade-swept area. Rohatgi (1996) attributes this assumption to von Karman's early work indicating a correspondence between wind flow and flow over flat plates. As is recognized, serious errors can be introduced by reliance on the power law to estimate average wind speed in the rotor swept-area. First, the power law has no theoretical basis for extrapolating wind speed within the boundary layer because it is not based on the basic principles of fluid mechanics and is instead derived empirically. Second, the power law is only considered valid during neutral conditions and over homogeneous, flat terrain. Finally, the power law does not acknowledge the possibility of variable wind shear across the rotor disk and its impact on turbulence.

A second on-site stability parameter, horizontal turbulence intensity (I_U), was calculated from SODAR, meteorological tower, and nacelle wind speed measurements using Eq (2),

$$I_U = \frac{\sigma_U}{U(z)} \tag{2}$$

where σ_U is the standard deviation of the mean horizontal wind speed (U) at height z. I_U was calculated for all nine measurement heights in the rotor disk using SODAR data, at heights of 40, 50 and 80 m using meteorological tower cup anemometer measurements, and at 80 m using the nacelle-mounted cup anemometer. Turbulence intensity is a function of atmospheric stability and surface roughness. In contrast to the wind shear exponent, α, which measures the wind shear that may produce turbulence, the turbulence intensity, I_U, directly measures turbulence

fluctuations of the lower boundary layer. High I_U magnitudes ($I_U > 20\%$) indicate that a larger proportion of the wind energy is composed of turbulent flow while low I_U values ($I_U < 10\%$) indicate laminar flow with less turbulence. I_U is a statistical descriptor of the overall level of turbulence, and therefore makes no quantitative distinction between thermal-produced turbulence (e.g., caused by convective cells in the mixed layer or buoyant air parcels near the surface) and shear-produced turbulence (e.g., caused by frictional drag along a rough, ground surface or strong shear just below a nocturnal low level jet). Additional high frequency measurements are required to quantify the source of turbulence, as in Piper and Lundquist (2004). Related to turbulence intensity, turbulence kinetic energy (*TKE*, $m^2\ s^{-2}$) was calculated from the 3-axis velocity SODAR data,

$$TKE = \frac{1}{2}(\overline{u'^2} + \overline{v'^2} + \overline{w'^2}) \tag{3}$$

In Equation (3), $\overline{u'^2}$, $\overline{v'^2}$, and $\overline{w'^2}$ are variance in u, v and w directions and are interpreted as the average of the square of the turbulence part of the wind speed. *TKE* was calculated for each of the 19 SODAR measurement heights. When strong winds are present or during neutral conditions, *TKE* may be nearly constant or decrease slightly with height (Stull 1988). During the day, *TKE* generally increases with height until a maximum is found at the level where free convection dominates. At night, *TKE* often decreases rapidly with height from a maximum value found just above the surface. An exception to this typical nighttime behavior occurs when low-level jets or other elevated sources of turbulence such as breaking gravity waves are present. If nighttime *TKE* is generated at levels above the surface in a statically stable atmosphere and is transported downward, then this suggests the presence a LLJ (e.g., Mahrt et al. 2001, Mahrt and

Vickers 2002, Lundquist 2003) and maximum winds may be found at heights equal to the top of the rotor swept-area (100 to 120 m AGL) (Lundquist and Mirocha 2008).

In addition, a nearby university research station provided 3-axis wind velocity and surface heat flux data from a sonic anemometer (CSAT3, Campbell Scientific Inc., Logan, Utah) during the study period from which the Obukhov length stability parameter was calculated. A sonic anemometer is a fast-response (sampling rate of 20 Hz), multi-axis wind sensor which measures the mean component of horizontal (u and v) and vertical (w) wind speed as well as the fluctuations from the mean (u', v' and w') which give information about the structures of organized turbulence. The off-site research station has some localized differences from the wind farm: its fetch includes flatter terrain and data indicate a slightly lower estimate of surface roughness, but the wind is consistently from the same direction. The Obukhov length (L, m) is a scaling parameter that is used as an indicator of atmospheric mixing conditions in the surface layer following Monin-Obukhov similarity theory (Monin and Obukhov 1954, Obukhov 1971, Nieuwstadt 1984, Stull 1988),

$$L = -\frac{\theta_v \cdot u_*^3}{k \cdot g \cdot \overline{w'\theta_v'}} \tag{4}$$

where θ_v is the virtual potential temperature (K), k is the von Karman constant (0.4), g is acceleration due to gravity (9.8 m s^{-2}), $\overline{w'\theta_v'}$ is the surface heat flux, and the friction velocity u_* is defined from the streamwise and crosswind turbulent momentum fluxes, $u_* = (\overline{u'v'}^2 + \overline{v'w'}^2)^{1/4}$. Due to the non-linear nature of L, and because L is often constant with height throughout the lower boundary layer, Eq (4) is commonly expressed as a non-dimensional scaling parameter $\frac{z}{L}$

where z is the height at which other variables are measured. The sign of the surface heat flux or buoyancy term in Eq (4) indicates whether the boundary layer is statically stable (negative buoyancy term) or statically unstable (positive buoyancy term). L or $\frac{z}{L}$ is defined as a negative quantity under convective or statically unstable conditions (heat flux is directed away from the surface), positive under statically stable conditions (heat flux is directed towards the surface), and approaches zero (no net buoyancy effects) under neutral conditions. A physical interpretation of the Obukhov length is that L is proportional to the height (in meters) above the surface at which thermal-produced turbulence begins to dominate shear-produced turbulence.

3.3 Stability classifications

For each 10-minute averaging period, we described the boundary layer mixing conditions based on Obukhov length, L(surface), wind shear exponent, α (at various heights), turbulence intensity, I_U (80 m), and turbulence kinetic energy, *TKE* (80m), and classified the time period as belonging to one of five stability classes: strongly stable, stable, neutral (includes slightly stable and slightly convective), convective, or strongly convective. The L, α, I_U, and *TKE* criteria for each of the five stability regimes are given in Table 2. The frequency of very stable or stable – to neutral – to convective or very convective periods was 36:27:37 during Winter (W), 51:30:19 during Spring (Sp), 57:22:21 during Summer (Su), and 34:26:40 during Autumn (A). Stable or very stable conditions were present during nearly all of the nighttime hours in the spring and summer months.

Stability class	L (m)	α	I_{U_80}	TKE_{80} ($m^2 s^{-2}$)	Boundary layer properties	Frequency			
						W	Sp	Su	A
strongly stable	$0 < L < 50$	$\alpha > 0.3$	$I_U < 8\%$	$TKE < 0.4$	Highest shear in swept-area, nocturnal LLJ may be present, little turbulence except just below the LLJ	11%	19%	22%	4%
stable	$50 < L < 200$	$0.2 < \alpha < 0.3$	$8\% < I_U < 10\%$	$0.4 < TKE < 0.6$	High wind shear in swept-area, low amount of turbulence	25%	32%	35%	30%
neutral	$L > 200$ or $L < -300$	$0.1 < \alpha < 0.2$	$10\% < I_U < 20\%$	$0.6 < TKE < 1.0$	Generally strongest wind speeds throughout the blade swept-area	27%	30%	22%	26%
convective	$-300 < L < -15$	$0.0 < \alpha < 0.1$	$20\% < I_U < 30\%$	$1.0 < TKE < 1.4$	Lower wind speeds, low shear in swept-area, high amount of turbulence	17%	15%	14%	20%
strongly convective	$-15 < L < 0$	$\alpha < 0.0$	$I_U > 30\%$	$TKE > 1.4$	Lowest wind speeds, very little wind shear in swept-area, highly turbulent	20%	4%	7%	20%

Table 2: Stability classifications for the four stability parameters (Obukhov length, wind shear, turbulence intensity, and turbulence kinetic energy), general atmospheric conditions, and frequency of occurrence during the data period. Wind shear, turbulence intensity and turbulence kinetic energy thresholds are based on the SODAR wind velocity data.

The stability thresholds listed in Table 2 are largely based on published values, although the criteria have been modified slightly according to the range of atmospheric conditions observed at this wind farm. The Obukhov thresholds are based on stability classifications given by Panofsky and Dutton (1984), and are similar to those used by van Wijk et al. (1990) in a study of offshore wind profiles and Sathe and Bierbooms (2007) in their assessment of turbine damage induced by atmospheric stability effects. The wind shear thresholds are based on work by van den Berg (2008) and Walter et al. (2009), although we defined a slightly lower threshold for strongly stable conditions (van den Berg (2008) uses $\alpha > 0.4$). Our turbulence intensity thresholds appear to be more site-specific than L or α and a review of other studies (Elliott and Cadogan 1990, Langreder et al. 2004, Tindal et al. 2008, Rareshide et al. 2009) suggests that most turbulence intensity thresholds are site-specific. For example, Rareshide et al. (2009)

defined just two stability classes based on a low turbulence threshold (I_U = 5 to 11%) and high turbulence threshold (I_U = 11 to 17%), while we defined five I_U stability classes including one which describes a neutral atmosphere using intermediate values of turbulence intensity (10% < I_U < 20%). In comparison, Tindal et al. (2008) examined what they described as a low turbulence intensity wind farm and subsequently defined the following I_U thresholds: low turbulence (0% < I_U < 5%), medium turbulence (5% < I_U < 10%), and high turbulence (10% < I_U < 15%). Most similar to our site, Elliott and Cadogan (1990) at a West Coast wind farm defined the following I_U thresholds, from low turbulence to high turbulence: 0 to 5%, 5 to 10%, 10 to 15%, and 15 to 30%. The *TKE* thresholds are based on boundary layer campaign data found in Stull (1988).

3.4 Equivalent wind speed

Because hub-height wind speeds may not represent the flow across an entire rotor disk or blade-swept area, a rotor-averaged wind-speed is often calculated when wind profiles across the rotor disk are available (Elliot and Cadogan 1990). High spatial resolution measurements from SODAR (10 m intervals from 40 to 120 m AGL) allow us to calculate a rotor-averaged wind speed or "equivalent" wind speed using Eq (5) (Wagner et al. 2009),

$$U_{equiv\_SODAR} = \frac{2}{A}\int_{H-r}^{H+r} U(z)(r^2 - H^2 + 2Hz - z^2)^{1/2}\,dz \tag{5}$$

where U_{equiv_SODAR} is the weighted or "equivalent" wind speed in the rotor swept-area as measured by the SODAR, A is the area of the turbine rotor (m^2), $U(z)$ is the mean wind speed (m s^{-1}) at height z (m), r is the radius of the rotor swept area (m), H is the hub-height (m) and z is the

measurement height (m). The equivalent wind speed is a more accurate estimate of the energy available to the rotor blades than hub-height wind speed. Following de Vries (1978) and Wagner et al. (2009) and theory presented in Rohatgi and Barbezier (1999) and Gottshall and Peinke (2008), we further modify Eq (5) to take into account that the instantaneous wind speed is a composite of the mean wind speed and turbulence. The interaction between turbulence and turbine performance is poorly understood although from a theoretical point of view, turbulence is additional energy in the wind, energy which is not quantified by using the mean wind speed alone (Rohatgi and Barbezier 1999). Turbulence encountered by the rotor is now accounted for in the $U_I(z)$ term in (Eq 6),

$$U_{equivTI\_SODAR} = \frac{2}{A}\int_{H-r}^{H+r} U_I(z)(r^2 - H^2 + 2Hz - z^2)^{1/2}\,dz \tag{6}$$

where $U_I(z)$ is calculated using the derivation of the average energy flux, (Eq 7),

$$U_I(z) = \sqrt[3]{U(z)^3(1+3I_U{}^2)} \tag{7}$$

Eqs (5 and 6) calculate a rotor-averaged wind speed which takes wind shear into account, while Eq (6) additionally includes turbulent energy making it a “true-flux” equivalent wind speed (Wagner et al. 2009).

Finally, the SODAR system is not co-located with the turbines used in this study, and in fact is often 3 km from the turbines discussed here. This distance makes it difficult to justify using the SODAR equivalent wind speed in the turbine power curves directly. Therefore, we make the assumption that the difference between the hub-height wind speed (SODAR 80 m) and the equivalent wind speed (Eq 5 or 6) could be considered a constant value (over a 10 minute

period) across the wind farm. The nacelle wind speeds are adjusted using Eq (8) to account for the difference between SODAR hub-height and SODAR equivalent wind speed (shown here using the "true-flux" equivalent wind speed),

$$U_{equivTI\_nacelle} = U_{nacelle} + (U_{equivTI\_SODAR} - U_{80\_SODAR}) \quad (8)$$

If the SODAR equivalent wind speed and the SODAR hub-height wind speed are identical for a ten-minute period, then there is no adjustment and $U_{equivTI\_nacelle} = U_{nacelle}$.

3.5 Comparison of available wind speeds

Access to a robust network of meteorological towers, SODAR, and nacelle wind data provides a number of ways to quantify the amount of wind energy available to the turbines. This section compares four methods of estimating wind speed in the rotor disk: (1) nacelle wind speed, (2) SODAR hub-height wind speed, (3) SODAR "true-flux" equivalent wind speed (Eq 7), and (4) nacelle-adjusted "true-flux" equivalent wind speed (Eq 8). Figure 1 shows that the frequency distribution of spring and summer winds is shifted towards lower wind speeds when the nacelle wind speed data are compared to the SODAR, perhaps due to turbine wake effects. This shift is most prevalent in the 6 to 10 m s^{-1} range when all turbulence classes are included (Fig 1a), but during times of only high turbulence becomes most noticeable at the lower end of wind speeds (2 to 7 m s^{-1}) (Fig 1c). Taking into account any differences between the hub-height wind speed and the "true-flux" rotor-averaged wind speed did not eliminate the frequency shift between the two instruments, which suggests that the wind speed differences between the cup anemometer and SODAR are instrument-driven. There are also small but important wind speed differences between the hub-height wind speed and "true-flux" equivalent wind speed, which are evident in both the nacelle and SODAR data. Differences between the 80 m and rotor-averaged

wind speed are most acute for wind speeds between 7 and 12 m s^{-1}, which is a critical range in the power performance curves of these turbines.

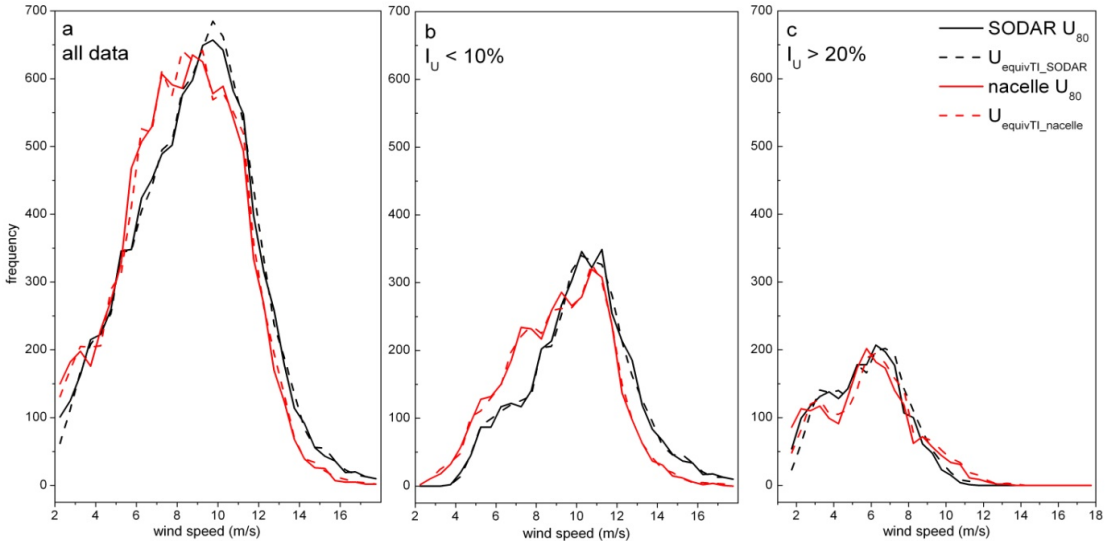

Figure 1. Frequency distribution of 10-minute SODAR hub-height, SODAR "true-flux" equivalent, nacelle hub-height, and nacelle-adjusted "true-flux" equivalent wind speed for Turbine #1 during the spring and summer months. Data are from (a) all time periods, (b) periods of low turbulence, and (c) periods of high turbulence. The distribution of cup anemometer data are shifted to the left towards the lower wind speeds.

3.6 Evaluation of power performance

Ten-minute averages of nacelle-mounted cup anemometer wind speed (m s^{-1}) and power (kW) from six 80-m tall turbines enable the generation of power curves (electrical power output versus wind speed) for this site. We select leading-edge turbines to remove any effects that turbine-induced wakes may have on turbine power performance in this analysis. Also, the distance between any upwind obstacles, e.g., the 80 m meteorological tower, and a downwind turbine is checked to make sure that the turbine is no closer than four times the rotor diameter from the upwind obstacle (IEC 2003). Manufacturer power performance data were obtained and were used to make comparisons between observed power curves and the manufacturer standard power curves. The manufacturer power performance data assumed standard atmospheric

conditions, including an assumption of neutral stability and turbulence intensity between 10-15%. Air density corrections for the manufacturer power curves using on-site air pressure and air temperature did not make a significant difference and are not shown in this study. Power production from an individual turbine is expressed here in terms of the capacity factor,

$$CF = \frac{P_{i.t}}{P_{rated}} \times 100\% \tag{9}$$

where, $P_{i,t}$ is the actual power (kW) at time, i, at turbine, t, and P_{rated} is the maximum power yield (kW) of the turbine as determined by the manufacturer. A capacity factor of 100% would indicate that a turbine is producing a power yield equal to the maximum power rating. For comparison, modern wind farms in the U.S. have an average capacity factor of 35%, with the most efficient ones reaching annual averages of around 48% (Wiser and Bolinger 2009). In addition to capacity factor, individual turbine performance was also evaluated using the power coefficient, C_p,

$$C_p = \frac{2P_{i,t}}{\rho_a A_t U_{i,t}^3} \tag{10}$$

where, ρ_a is air density (kg m^{-3}), A_t is the area of the turbine rotor (m^2), and $U_{i,t}$ is the equivalent wind speed ($U_{equivTI\_nacelle}$) at time, i, at turbine, t. The power coefficient indicates how efficient the turbine is at converting wind energy into electricity. Theoretically, the maximum mechanical efficiency of a turbine is 59.3% and is known as the Betz limit (Betz 1966). More typically, turbines have maximum efficiencies approaching 40% to 45%. Here, CF and C_p were calculated for each 10-minute period.

4. Results

4.1 Seasonal wind speed and direction at the site

This wind farm had significant seasonal and diurnal variations in the mean wind speed. Wind speeds overall were higher at night than during the day and higher during the warm season than in the cool season (Figure 2). The largest seasonal wind speed variability occurred during the nighttime hours so that the average summer nighttime wind speed was twice as fast as in winter: mean hub-height wind speed was 5.4 m s^{-1} (winter) and 10.1 m s^{-1} (summer). Less seasonal variability was present during the daylight hours although daytime wind speeds also seasonally peaked during the warmer summer months. Diurnal variability was minimal during winter and autumn but significant during the summer and spring (Figure 3). At the 120 m height, mean wind speed varied by up to 7 m s^{-1} between daytime and nighttime in the summer but in the winter differed only 2 m s^{1}. Mean annual nighttime hub-height wind speed was 8.5 ± 2.8 m s^{-1} from SODAR and 8.3 ± 2.6 m s^{-1} from the meteorological tower. Mean annual daytime hub-height velocity was 6.5 ± 3.2 m s^{-1} from SODAR and 6.7 ± 3.0 m s^{-1} from the meteorological tower. The Pearson's correlation coefficient (r) between SODAR and meteorological tower hub-height wind speed was r = 0.87 during the day and r = 0.69 at night during the spring and summer months. The meteorological tower data showed greater height variability in the daytime wind speeds than the SODAR between heights of 50 m and 80 m although this may be an artifact of the 8 km distance between the two meteorological towers. The tower and SODAR were also not co-located and were separated by 3 km which explains some of the discrepancy between the two datasets.

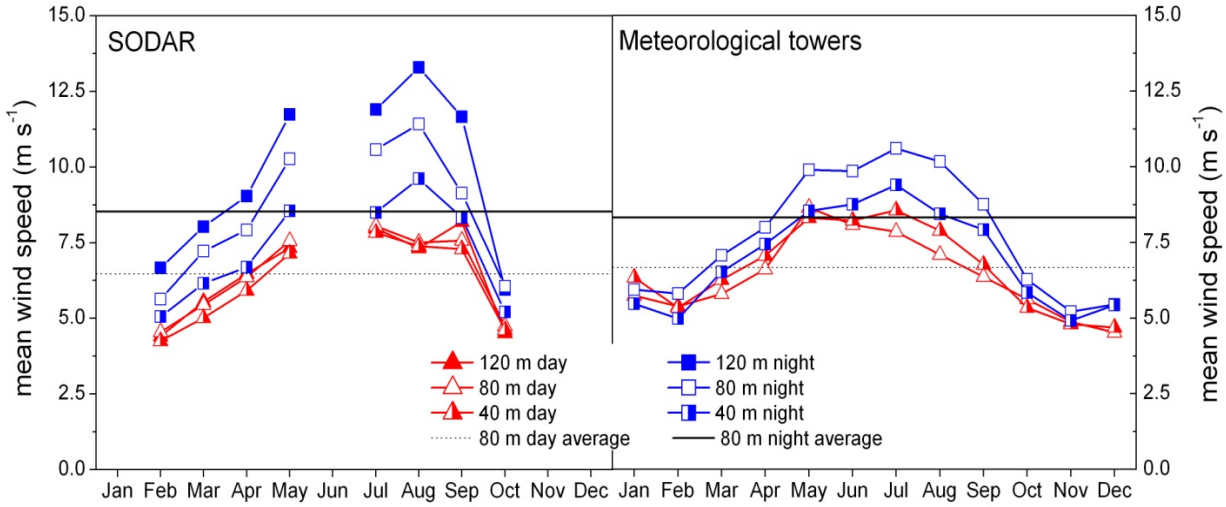

Figure 2: Monthly mean night and day wind speeds at 40 m, 80 m and 120 m heights from SODAR and the meteorological towers show strong seasonality. The mean nighttime and daytime hub-height velocities (80 m) are an average of all months except for Jan., June, Nov., and Dec.

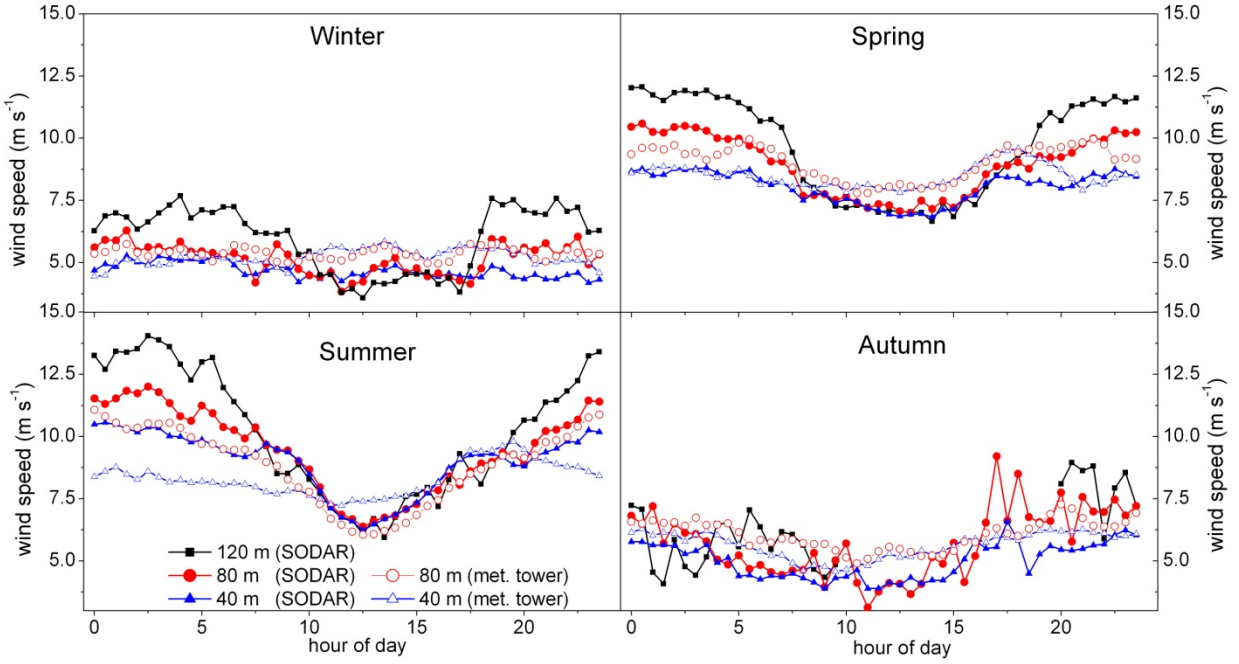

Figure 3: Seasonal diurnal plots of 40 m, 80 m, and 120 m mean wind speed show a strong diurnal signal during spring and summer. Diurnal variation in wind speed is lower at the 40 m height than at 120 m above the ground and lower during the winter and autumn months at all heights than during the summer and spring.

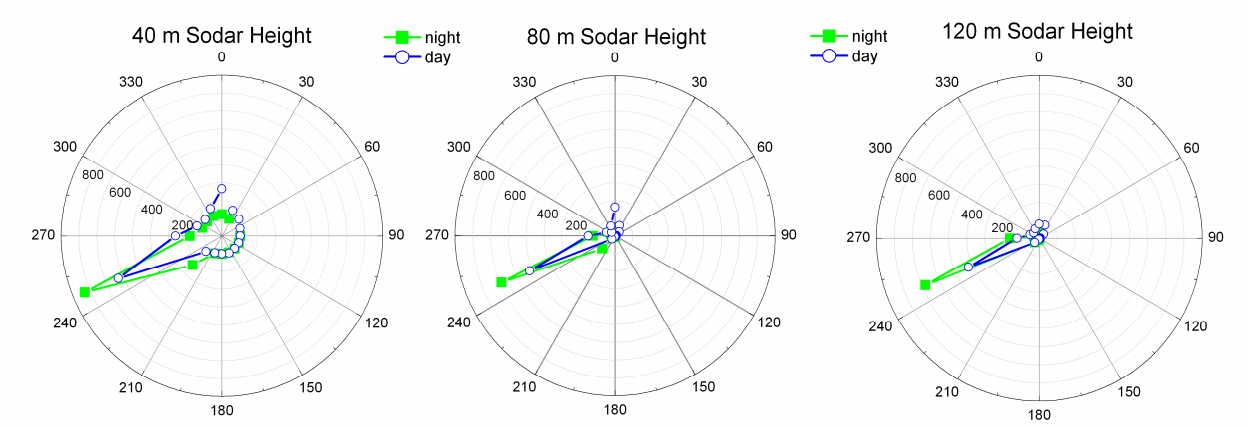

Figure 4: Frequency plots of nighttime/daytime wind direction for 40 m, 80 m and 120 m wind velocities during the spring show that winds are predominantly from the WSW at this wind farm.

In contrast to wind velocity, wind direction measurements at the 40 m, 80 m and 120 m heights show a small degree of temporal (night versus day) and spatial (vertical height) variability throughout the year. Average wind roses for the spring months are shown in Figure 4. Nighttime winds were consistently from the west-southwest. Daytime winds were occasionally from the north but showed predominance in the west-southwest direction. On average, there was a small amount of directional shear ($\frac{\Delta direction}{\Delta height}$) across the entire blade swept area, with greater shear occurring in the lower half of the swept area (40 m to 80 m) than in the upper half (80 m and 120 m) during the daylight hours. Figure 4 indicates that changes in wind direction with height and time of day are not a significant concern at this wind farm.

4.2 Stability parameter analysis and comparison

The percentage of summer time periods defined as stable, neutral or convective by the Obukhov length, wind shear exponent (SODAR α_{40_120}), turbulence intensity (SODAR I_{U80} or nacelle I_{U80}), and turbulence kinetic energy (SODAR TKE_{80}) are shown in Figure 5. The

Obukhov length (Fig 5a, shown here as $\frac{z}{L}$) predicted that stable:neutral:convective conditions occurred in a 42:30:28 ratio. The SODAR-based stability parameters, α_{40_120} (Fig 5b), I_{U80} (Fig 5c) and TKE_{80} (Fig 5e) show high agreement with $\frac{z}{L}$, although the wind shear parameter predicted a slightly higher percentage of convective conditions. The nacelle-based turbulence intensity parameter (Fig 5d) shows poor overall agreement with the other stability parameters. Nearly 90% of the summer (daytime and nighttime hours) was classified as stable or neutral by nacelle-based I_U while $\frac{z}{L}$ predicted stable or neutral conditions just 72% of the time.

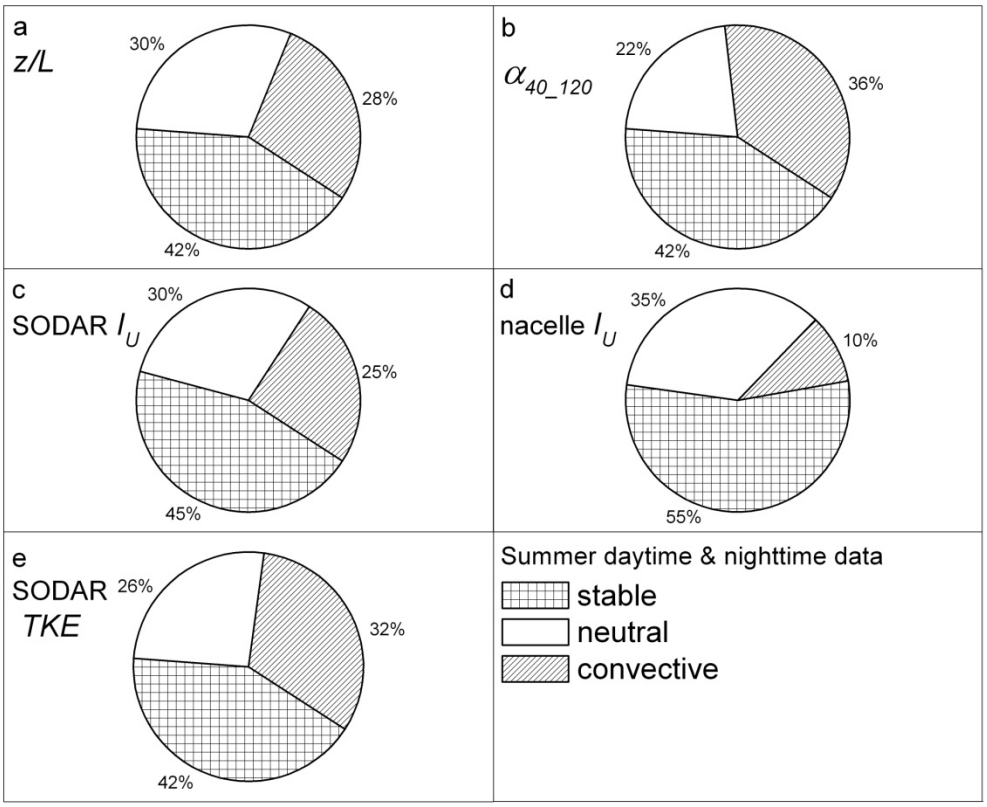

Figure 5: Percentage of summer time periods classified as stable, neutral or convective according to the four stability parameters: (a) normalized Obukhov length, (b) SODAR wind shear, (c) SODAR turbulence intensity, (d) nacelle turbulence intensity, and (e) SODAR turbulence kinetic energy. The stability parameter with highest agreement to $\frac{z}{L}$ is SODAR *TKE*.

Figures 6, 7, and 8 show the distribution of α, SODAR I_U, and *TKE* magnitudes for a range of $\frac{z}{L}$ stability bins. When $\frac{z}{L}$ indicated neutral conditions ($\frac{z}{L} = 0$), median (25th percentile) (75th percentile) α = 0.14 (0.06) (0.23), SODAR I_U=12% (9.7) (13.8), and *TKE* = 0.76 m^2 s^{-2} (0.54) (1.00). When $\frac{z}{L}$ indicated stable conditions ($\frac{z}{L} > 0$), median (25th percentile) (75th percentile) α = 0.31 (0.24) (0.36), SODAR I_U= 8.2% (7.3) (9.1), and *TKE* = 0.42 m^2 s^{-2} (0.31) (0.55). When $\frac{z}{L}$ indicated convective conditions ($\frac{z}{L} < 0$), median (25th percentile) (75th percentile) α = 0.02 (-0.04) (0.07), I_U= 25% (18) (43), and *TKE* = 1.2 m^2 s^{-2} (0.98) (1.38). The median values for α, SODAR I_U and *TKE* are well within the thresholds given in Table 2 for the three major stability regimes (stable, neutral or convective). Most of the 25th and 75th percentiles are also within the thresholds.

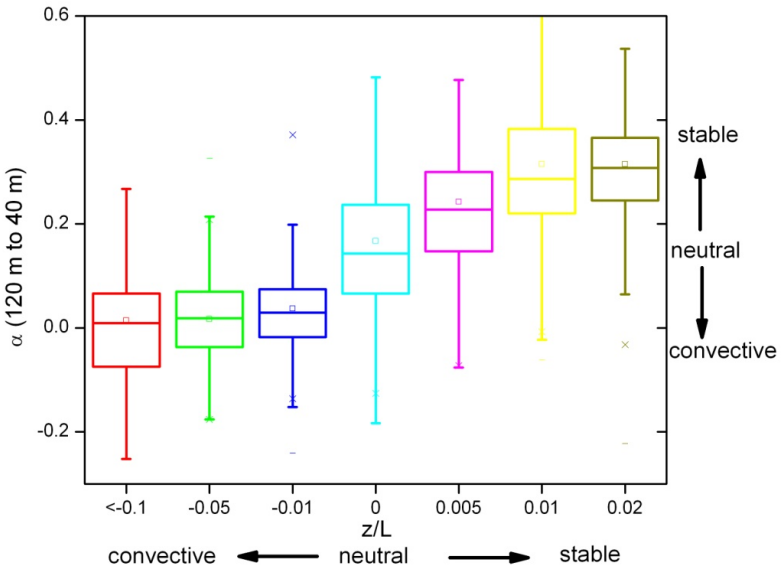

Figure 6: Histogram of 10-minute SODAR wind shear (α_{40_120}) data according to $\frac{z}{L}$ stability class. The box-plot histogram shows the mean (small square), median (horizontal line), 25th and 75th percentiles (bottom and top of the box), and 5th and 95th percentiles (lower and upper whisker line).

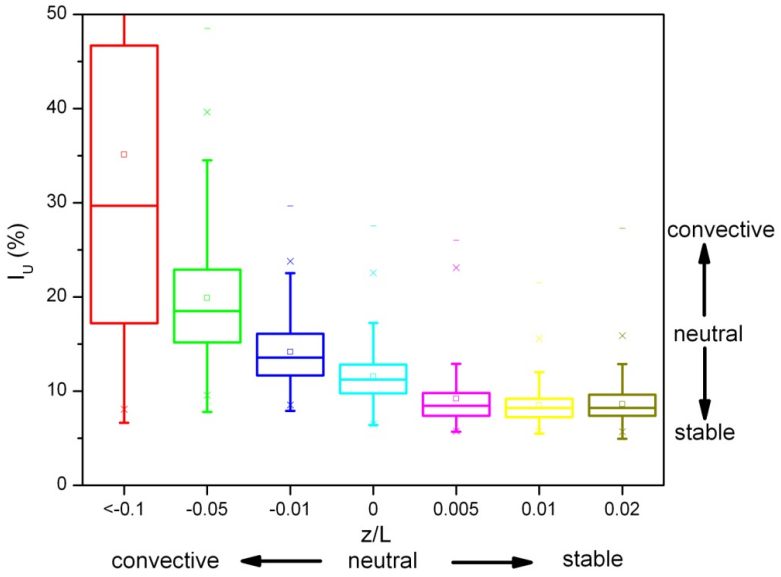

Figure 7: Histogram of 10-minute hub-height, SODAR turbulence intensity (I_U) data according to $\frac{z}{L}$ stability class. The box-plot histogram shows the mean (small square), median (horizontal line), 25th and 75th percentiles (bottom and top of the box), and 5th and 95th percentiles (lower and upper whisker line).

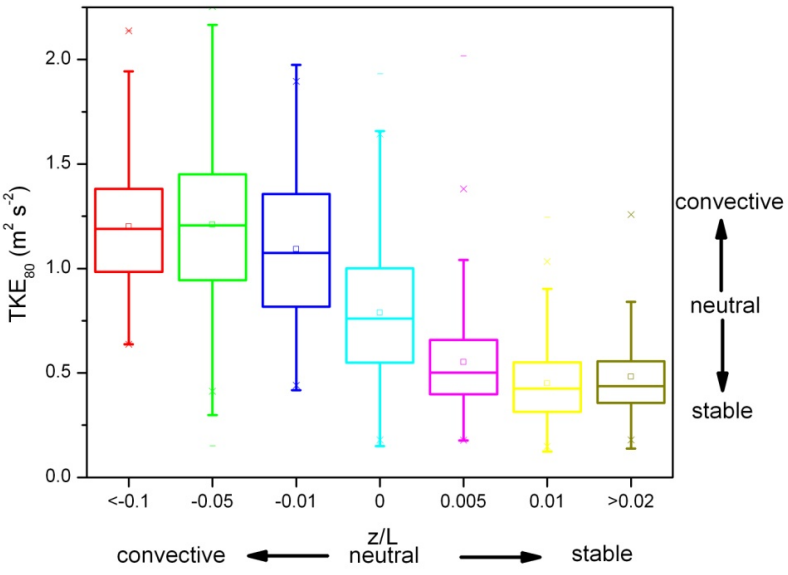

Figure 8: Histogram of 10-minute hub-height, SODAR turbulence kinetic energy (*TKE*) data according to $\frac{z}{L}$ stability class. The box-plot histogram shows the mean (small square), median (horizontal line), 25th and 75th percentiles (bottom and top of the box), and 5th and 95th percentiles (lower and upper whisker line).

As expected, each stability parameter (L, α, SODAR I_U, and TKE) indicated that daytime periods were mostly convective or near-neutral while nighttime periods were stable or slightly stable. Strongly stable conditions occurred at night more frequently during the warmer months than during autumn or winter. Figure 9 shows that wind shear across the entire rotor area (α_{40_120}) was, on average, greater than 0.2 at night and less than 0.1 during the day. Maximum α-values (0.3 to 0.5) were consistently observed on summer nights across the entire rotor swept-area. Also, on spring and summer nights, wind shear was on average much higher in the upper half of the swept area (80 m to 120 m) than in the lower half, possibly indicating the presence of low-level jet structures at heights above the top blade tip which do not penetrate to the lower half of the rotor. During the day, wind shear was generally higher in the lower half of the rotor disk (40 m to 80 m) than the upper half and α-values indicated a well-mixed boundary layer throughout the swept area with substantial surface drag occurring near the ground.

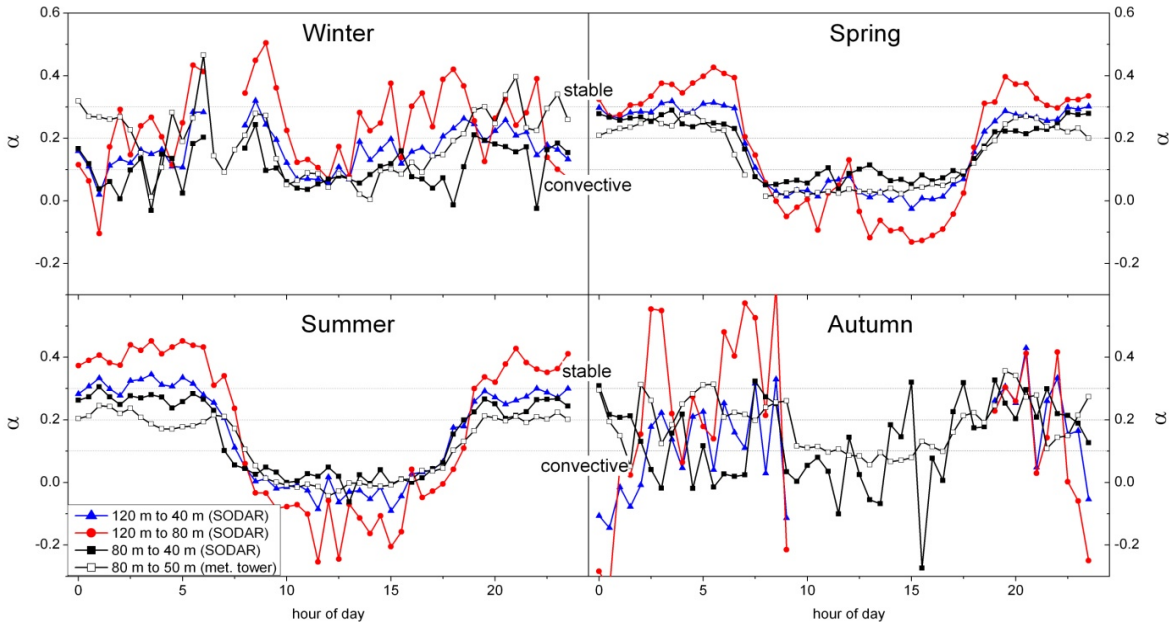

Figure 9: Diurnal plot of mean wind shear (α) between heights of 40-120 m, 80-120 m, 40-80 m, and 50-80 m AGL by season. The 50 m to 80 m α is based on cup anemometer measurements. The dotted lines indicate the SODAR-based α stability classifications from Table 2. Some hours are missing in autumn and winter panels due to periods of poor data recovery (e.g., low signal to noise ratio) at the 120 m height.

SODAR turbulence intensity was higher during the day than at night throughout the year, although Figure 10 shows that the diurnal variability in turbulence intensity at the 40 m, 80 m, and 120 m heights varied from season to season. The observed diurnal variability is similar to that found by Rareshide et al. (2009) at a site in the U.S. Great Plains, although this West Coast site showed that turbulence intensity was highest during the winter and autumn months (the rainy season) during both daytime and nighttime hours, while in the Great Plains, the summer months showed highest turbulence intensity. Figure 10 shows that average daylight 80-m horizontal turbulence intensity was lowest (mean I_U = 20%) during July and highest during October (mean I_U = 35%). Spring and summer nighttime I_U magnitudes indicate a strongly stratified boundary layer at night: average I_U at 40 m was 9.7 %, at 80 m was 8.2%, and at 120 m was 7.3%.

It is also evident from Figure 10 that the SODAR and cup anemometer measurements (at the meteorological tower and nacelle hub) measured different intensities of turbulence during the daylight hours, although both instrument platforms show a daytime increase in turbulence intensity compared to nighttime measurements. The cup anemometers measured much lower turbulence intensities during the daytime hours as compared to the strong daytime peak observed by the SODAR. For example, during summer midday hours at the 80 m height, mean SODAR I_U was 28% while the cup anemometer measured a mean value of 18% at the meteorological tower and 13% at the nacelle hub. Further analysis showed that the summer-time difference in I_U came largely from differences in the standard deviation of the 10 minute measurements. The cup anemometer σ_U was systematically lower than the SODAR σ_U measurement. For the same daylight hours, the average standard deviation of mean wind speed (σ_U) from the SODAR was 1.4 m s^{-1} while the cup anemometer measured σ_U = 0.88 m s^{-1} at the meteorological tower and 0.71 m s^{-1} at the nacelle. Observations of systematically low variance in cup anemometer

measurements have also been reported by Hölling et al. (2007) in a wind tunnel comparison study of anemometers.

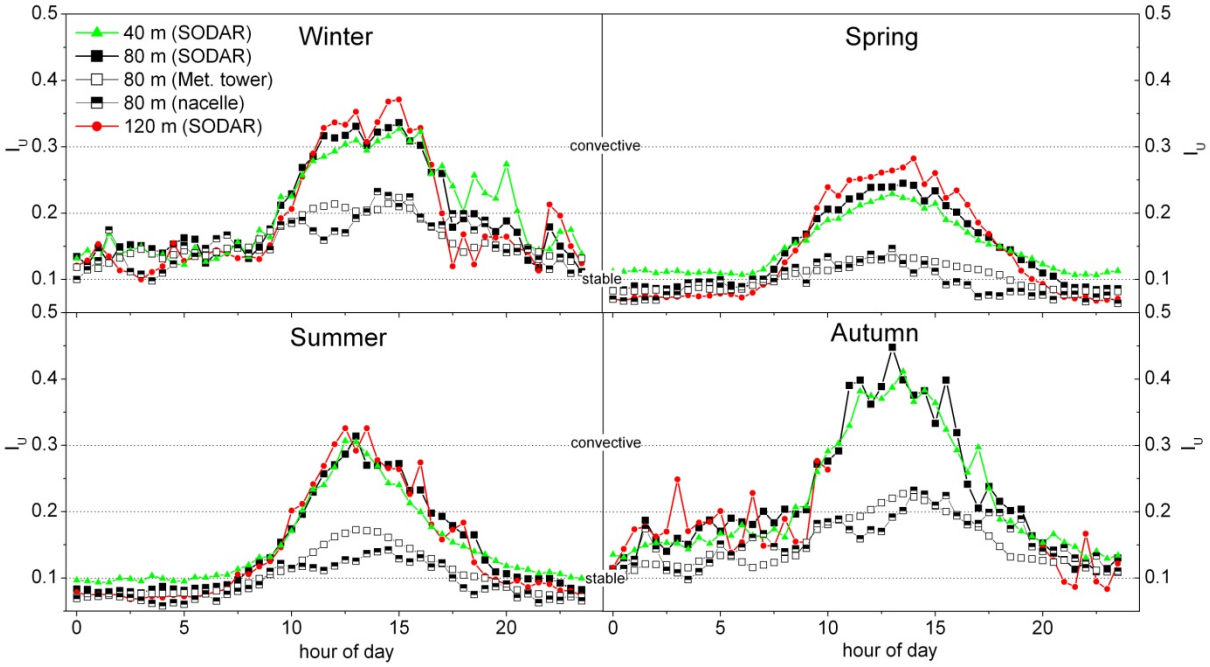

Figure 10: Diurnal plot of mean horizontal turbulence intensity at 40 m, 80 m and 120 m by season. The 80m I_U is based on three instrument locations: SODAR, meteorological tower, and the nacelle. Turbulence intensity is higher during the day than at night and highest during autumn afternoons and lowest during spring and summer nights. During the night turbulence intensity closer to the ground at 40 m is generally larger than at the 80 m or 120 m heights. The dotted lines indicate the SODAR-based I_U stability classifications from Table 2.

Figure 11 compares the cup anemometer I_U 10-minute data (meteorological tower and nacelle) to SODAR I_U for five days in August. Minimum turbulence intensity magnitudes were slightly lower (~ 0.02) in the cup anemometer dataset although much larger instrument differences were observed at higher I_U values. During this period, 16% of SODAR I_U data were above 20% while less than 1% of the cup anemometer I_U values reached 20%.

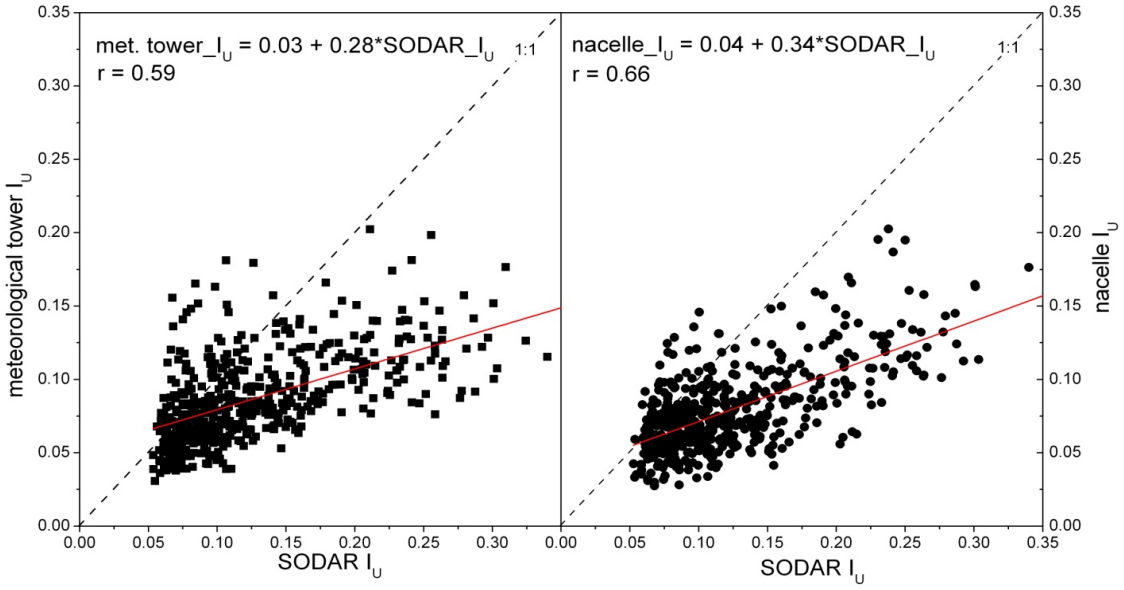

Figure 11: Meteorological tower-based I_U (80 m) (left panel) and nacelle-based I_U (80 m) (right panel) versus SODAR-based I_U (80 m) for five days during the summer period (Aug. 1- 5) shows a strong bias towards larger SODAR turbulence intensity values. Maximum cup anemometer (met. tower and nacelle) I_U reaches just 20% while SODAR I_U maxima reach 35%.

4.3 Stability influence on wind velocity and turbulence profiles

We used the SODAR-measured turbulence intensity at 80 m to further investigate the effects of stability regime (convective versus neutral versus stable) on the rotor disk wind profiles. Figure 12 shows that, in addition to seasonal variability in mean wind speed, stability-correlated variability was evident at all times of the year although it was strongest during spring and summer. Peak wind speeds at all heights (40 m to 120 m) were typically observed during stable conditions, except during the winter period, when the highest wind speeds were observed during neutral conditions. Maximum wind speeds at hub-height and above were observed during strongly stable and stable conditions; during spring and summer, the stable wind maxima exceeded neutral wind maxima by 2 to 3 m s^{-1}. Hub-height wind speed and wind shear were significantly lower ($P < 0.05$) during convective or strongly convective conditions than during stable regimes for all seasons.

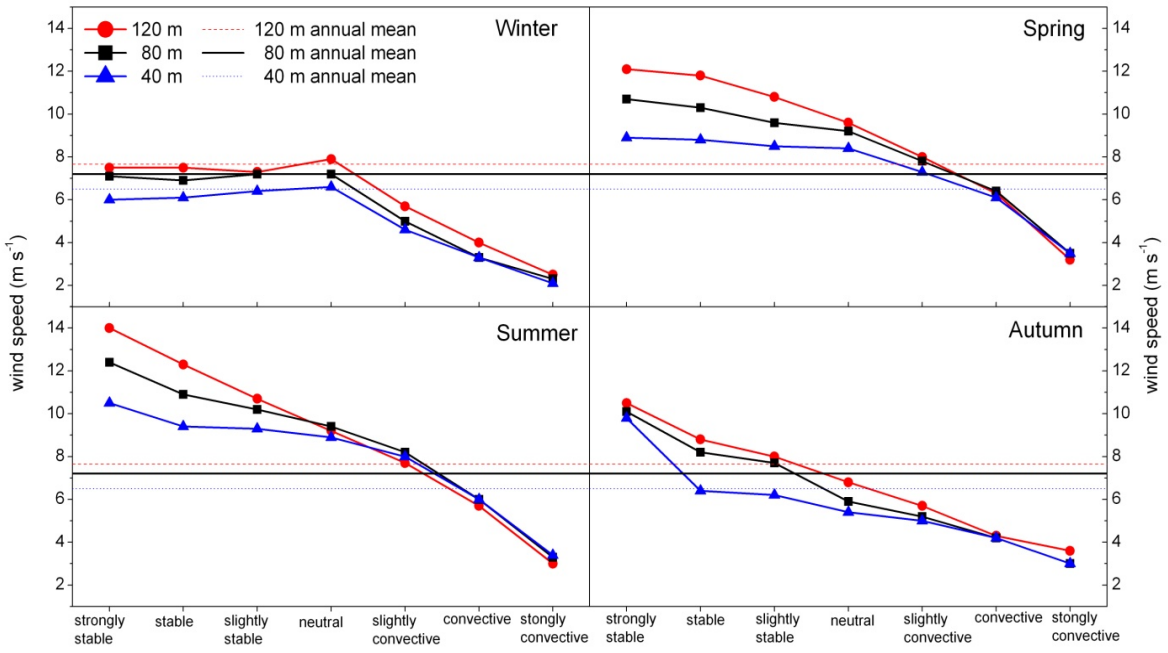

Figure 12: Wind speed across the rotor diameter (40, 80 and 120 m) according to I_U -defined stability class and month. Also plotted is annual mean wind speed at each height.

During autumn (not shown) and winter (not shown), influences of atmospheric stability on vertical profiles of mean wind speed were less apparent than during the warmer months at this site. Average autumn and winter wind velocity profiles (up to 100 m AGL) were accurately predicted by the 1/7th power law expression regardless of atmospheric stability. The spring (Figure 13) and summer (Figure 14) vertical profiles of mean wind velocity and *TKE* show a stronger dependency on atmospheric stability. Significant differences between measured and extrapolated (using α = 1/7) wind velocity occurred during both stable and convective conditions.

Figure 13a shows that during stable spring-time conditions, the power law expression underestimated wind speed in the upper half of the rotor by 1 to 1.5 m s^{-1} and overestimated wind speed in the lower half of the rotor by 0.5 to 1 m s^{-1}. In contrast, during convective

conditions, wind speed was overestimated in the top half of the rotor by 1.0 to 1.5 m s^{-1}, underestimated in the lower half by 0.3 m s^{-1}, and wind shear was much less than 1/7. *TKE* decreased with height (up to 100 m) during stable conditions, was nearly constant with height during neutral conditions, and increased rapidly with height during convective conditions (Fig 13b). The largest changes in *TKE* with height were observed in the lower half of the rotor regardless of stability regime. Summer-time vertical profiles of mean wind speed were similar to those observed in the spring except that we observed stronger stability influences during convective conditions (Fig 14a). During convective conditions, wind speed was overestimated in the top half of the rotor by 1.5 to 2.0 m s^{-1} and underestimated in the lower half of the rotor by 0.5 m s^{-1}.

Increasing wind speeds aloft (100 to 120 m) indicated the possible presence of low-level jets, although we did not observe evidence of increased turbulence induced by shear at heights just below the wind maxima (Figures 13b and 14b), such as a significant peak in *TKE* just below the LLJ. The lack of *TKE* maxima at ~100 m AGL may be due to the monthly averaging approach, which could have eliminated evidence of LLJs if they did not occur regularly each night.

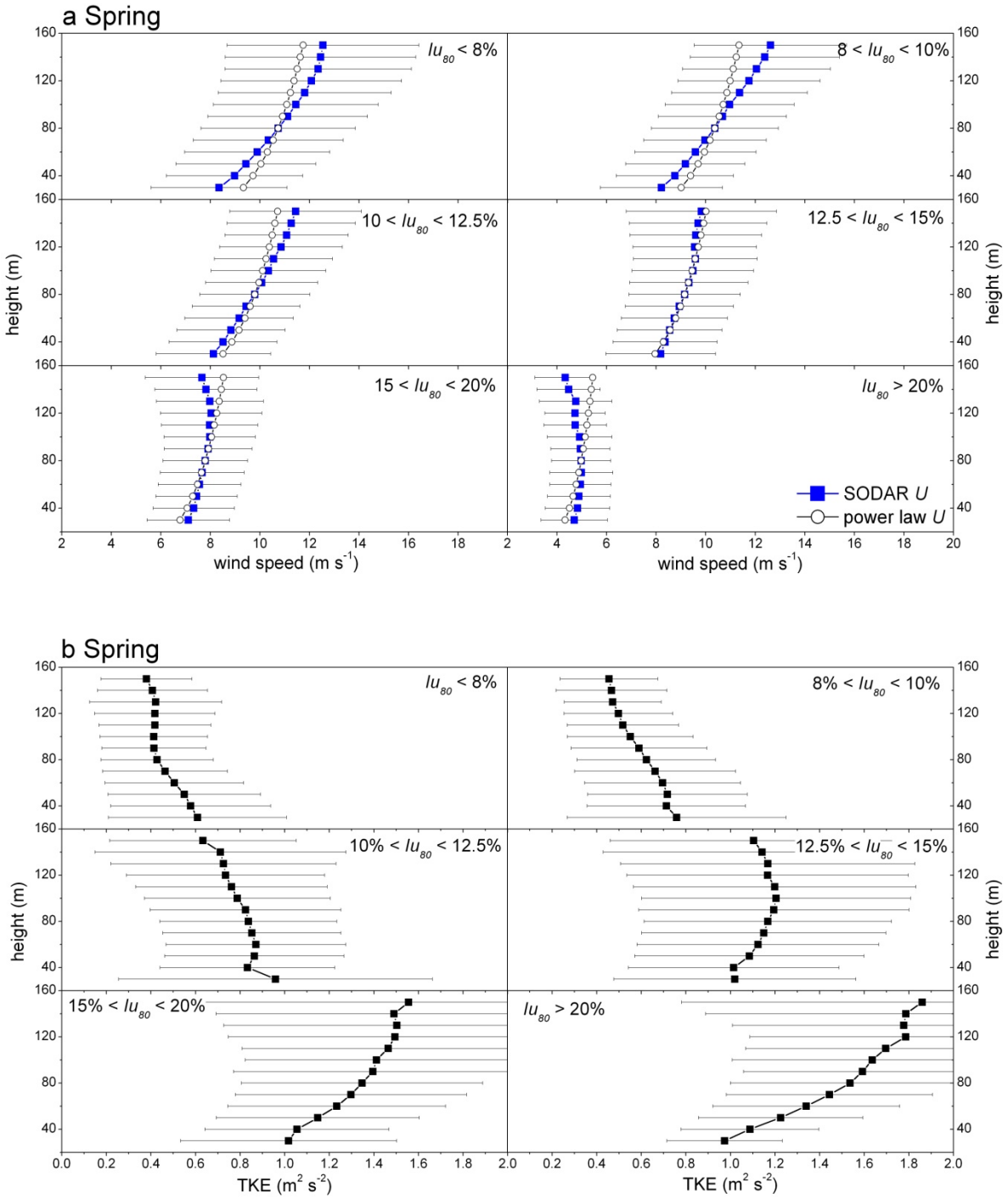

Figure 13: Spring vertical profiles (30 m to 150 m) of SODAR mean wind speed (a) and turbulence kinetic energy (b) during very stable (I_U < 8%), stable (8% < I_U < 10%), slightly stable (10% < I_U < 12.5%), neutral (12.5 % < I_U < 15%), slightly convective (15% < I_U < 20%), and convective (I_U > 20%) conditions. The error bars are ± one standard deviation from the mean. Also plotted is the predicted wind speed profile (open circles) based on the 1/7th power law (α = 0.144) and 80 m wind speed.

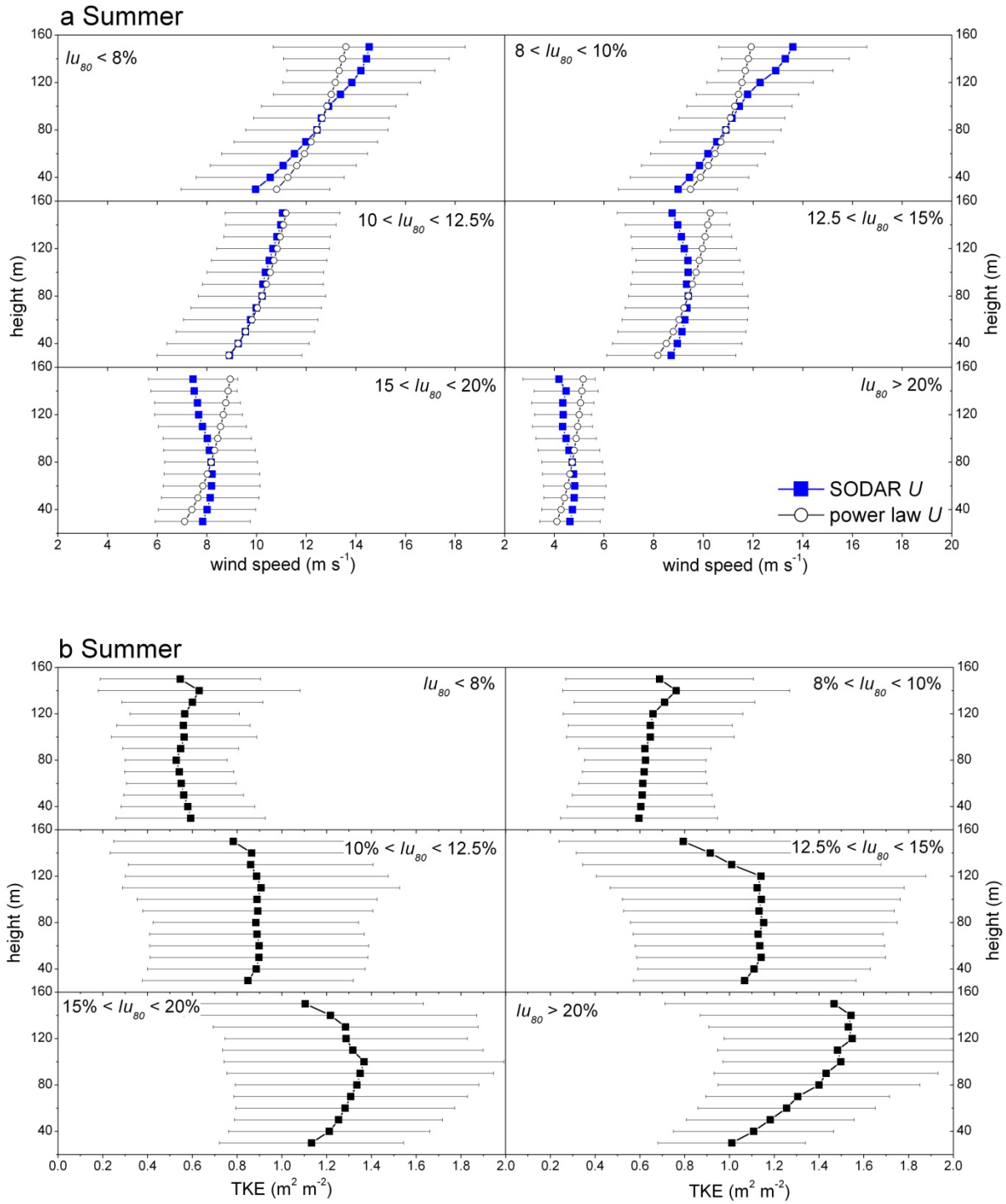

Figure 14: Summer vertical profiles (30 m to 150 m) of SODAR mean wind speed (a) and turbulence kinetic energy (b) during very stable (I_U < 8%), stable (8% < I_U < 10%), slightly stable (10% < I_U < 12.5%), neutral (12.5 % < I_U < 15%), slightly convective (15% < I_U < 20%), and convective (I_U > 20%) conditions. The error bars are ± one standard deviation from the mean. Also plotted is the predicted wind speed profile (open circles) based on the 1/7th power law (α = 0.144) and 80 m wind speed.

4.4 Seasonal power output at an individual turbine

This wind farm experiences two distinct wind power seasons: autumn/winter and spring/summer, as determined by the regional climatology. The rainy, winter season brings months with lower wind speeds and lower capacity factors than average. Greater power production occurs during the warm, dry season. Seasonal average capacity factors at Turbine #1 during winter, spring, summer, and fall were respectively 22%, 53%, 58%, and 23% (Figure 15). Figure 16 shows that greater amounts of power were produced during the nighttime hours in summer and spring (corresponding with higher wind speeds in the top of the rotor as shown in Figure 2) than during autumn and winter, while a smaller seasonal increase was also observed during the daytime hours. Average nighttime (22:00 – 2:00) capacity factor was 23% in winter, 63% in spring, 77% in summer, and 26% in autumn at Turbine #1. Average midday (10:00 – 14:00) capacity factor was 16% in winter, 40% in spring, 32% in summer, and 14% in autumn. Capacity factors were on average 14% higher on summer nights than on spring nights and 8% lower during daylight hours in the summer compared to spring. These capacity differences are explained by higher wind speeds on summer nights and on spring days.

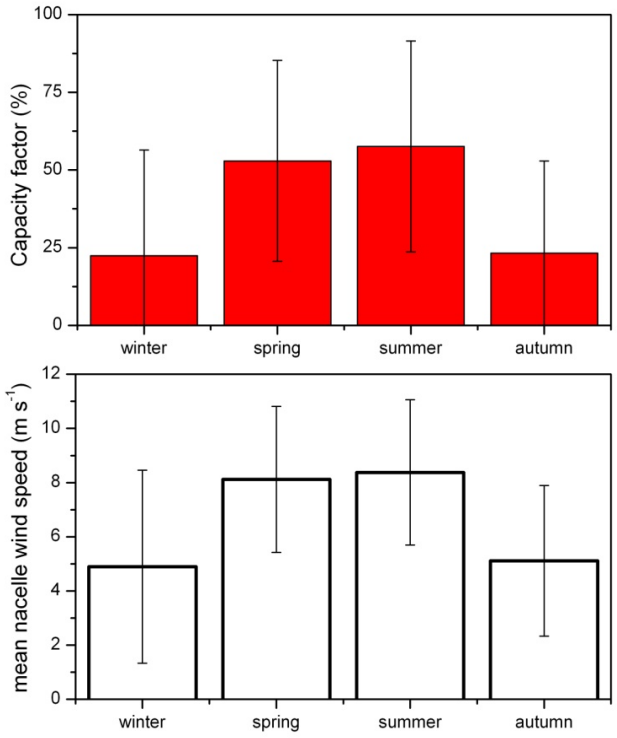

Figure 15: Seasonal mean (± one standard deviation) capacity factor and nacelle wind speed for a single turbine, Turbine #1. Wind speeds during the spring and summer were on average 3 m s^{-1} higher than during the cooler months, while the capacity factors were on average 30-36% greater.

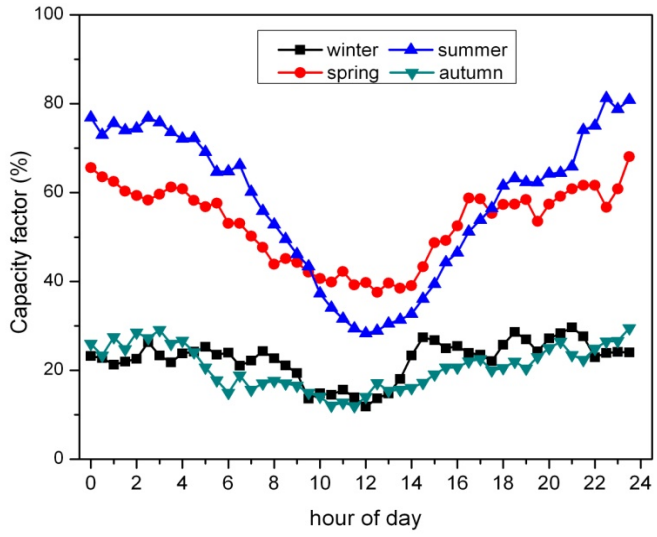

Figure 16: Mean diurnal capacity factor at Turbine #1 by season shows large power differences at night between spring/summer periods and winter/autumn periods which approach 50%. Smaller power differences are also observed during the daytime hours.

4.5 Wind speed representation in power curves

Power curves from the manufacturer conventionally show power collection as a function of hub-height wind speed. Recent work (Antoniou et al. 2007, Wagner at al. 2009) has shown the utility of considering a wind speed representative of the entire rotor area (Eq 5, above) or of considering a wind speed "corrected" for the influence of turbulent kinetic energy (Eq 6, above). Remote sensing observational platforms such as SODARs or LIDARs are required to provide the data necessary to represent winds and turbulence over the entire rotor disk, but often these remote sensing units are not co-located with the turbines. To examine these two issues, Figure 17 illustrates the limitations of using non co-located SODAR wind speed in the power curve and the improvement (in terms of matching the manufacturer power curve) from using nacelle-adjusted "true-flux" equivalent wind speed (Eq 8, above) instead of nacelle hub-height wind speed. Using $U_{equivTI\_nacelle}$ in the power curves increased the Pearson's correlation coefficient from r = 0.88 (power versus SODAR hub-height wind speed) to r = 0.95. The standard deviation of residuals (measured capacity factor – expected capacity factor) also shows less variation when power is plotted as a function of $U_{equivTI\_nacelle}$ ($\sigma_{residual}$ = 6.5%) instead of $U_{nacelle}$ (hub-height) ($\sigma_{residual}$ = 6.0%). At this wind farm, the nacelle-adjusted "true-flux" equivalent wind speed appears to generate the most accurate power curves. Simulations done by Wagner et al. (2009) using tall turbines have also shown that power output has a more significant correlation to "true-flux" equivalent wind speed than to hub-height wind speed.

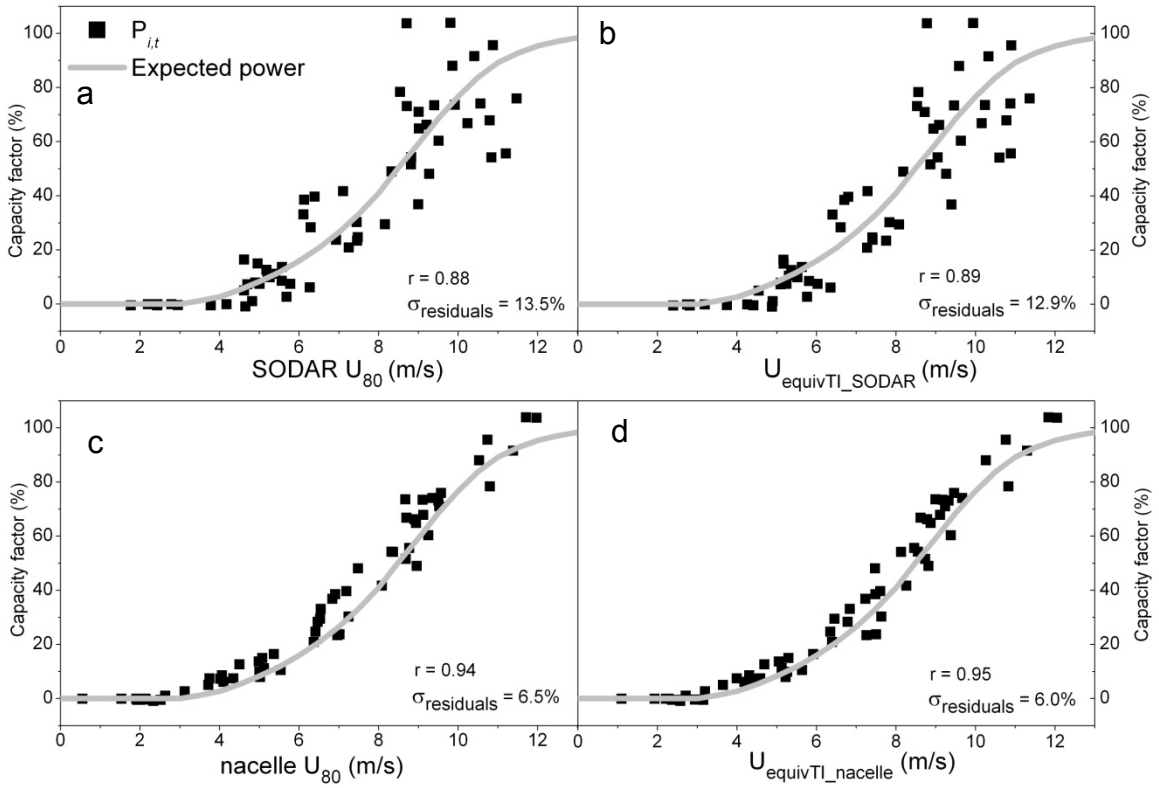

Figure 17: 10-minute power (shown as capacity factor) and wind speed data from a single, typical summer day show the best fit between $U_{equivTI\_nacelle}$ and power. Wind speeds plotted are (a) SODAR hub-height wind speed , (b) SODAR "true-flux" equivalent wind speed, (c) nacelle hub-height wind speed, and (d) nacelle-adjusted "true-flux" equivalent wind speed (d). The nacelle and power data are from Turbine #1. Also plotted is the expected or manufacturer's power curve.

4.6 Stability parameter influence on power performance

In the next four sections, power performance at an individual turbine (Turbine #1) and for a subset of turbines (in 4.6.3) is examined for stability-effects by separating the 10-minute power data into periods of strongly stable or stable, convective, or strongly convective conditions. The power curves are shown for the spring and summer months only since the wind speed profiles do not significantly vary amongst stability regimes during the winter and autumn months. The first analysis (4.6.1) uses nacelle-based turbulence intensity (I_U) to define atmospheric stability while sections 4.6.2 through 4.6.4 use SODAR-based stability parameters: wind shear (α), hub-height I_U, and turbulence kinetic energy (*TKE*). The stability thresholds and corresponding stability

regimes are the same as those listed in Table 2. In each of the following sections, power performance is evaluated by plotting (1) mean capacity factor as a function of wind speed in stability-stratified power curves and (2) normalized power as a function of stability regime for three wind speed ranges. Normalized power is the ratio of actual power generated at time, *i*, by turbine, *t*, to the expected amount of power (as given by the manufacturer) for the wind speed at time, *i*. In the power curves figures, some data points are missing (e.g., power during high wind speeds for convective conditions) because there were too few 10-minute data to statistically represent the 0.5 m s^{-1} wind speed bin. The wind speed in all of the figures is the "true-flux" equivalent wind speed. By inspection of power segregated by atmospheric stability parameters (Figs 18-26), we can discern the utility of those atmospheric stability parameters to suggest turbine power performance in different stability regimes.

4.6.1 Stability parameter: *nacelle* I_U

Figure 18 shows the summer performance curve for Turbine #1 where stability was determined by the nacelle-based (cup anemometer) turbulence intensity and the power data were stratified into stable or strongly stable periods, slightly convective periods, and convective periods. Too few data points were available during strongly convective conditions to include in Figure 18. For the most part, the turbine produced as much power as expected during each stability regime. There are small power differences between the power curves for Turbine #1 and the manufacturer's power curve and also between the stability-stratified power curves. These power differences are less than 10% and occurred when the "true-flux" equivalent wind speed was between 6.5 and 8.5 m s^{-1}.

Figure 19 examines if wind speed has any effect on the role that atmospheric stability (based on nacelle I_U) has on power performance by examining the stability-stratified capacity factors for three wind speed ranges: 4.5 to 6.5 m s^{-1}, 6.5 to 8 m s^{-1}, and 8 to 10.5 m s^{-1}. In this figure, each of the 10-minute power data is normalized by the expected power (according to the manufacturer's power prediction) for the corresponding 10 minute wind speed. The nacelle I_U-stratified power data show that the turbine slightly under-performed during slightly convective and convective conditions during moderate wind speeds although the differences are not significant. During very low and very high wind speeds, on the other hand, convective conditions actually led to slightly higher power production than expected. This finding differs with previous stability studies (e.g., Elliott and Cadogan 1990, Rareshide et al. 2009). For example, Rareshide et al. (2009) found competing effects of turbulence intensity in different parts of the power curve; namely that increasing turbulence intensity increases the power output in the concave region of the power curve (wind speeds are between 4 and 8 m s^{-1}) and decreases the machine's power in the convex region of the power curve (wind speeds are above 8 m s^{-1}). The nacelle-based cup anemometer is influenced by the turbine's own extraction of power from the atmosphere as well as the possible distortion of flow through the rotor disk and around the nacelle hub. We suggest that the use of a nacelle-based I_U (as in Figure 18) can mask the actual effects of turbulence on power performance.

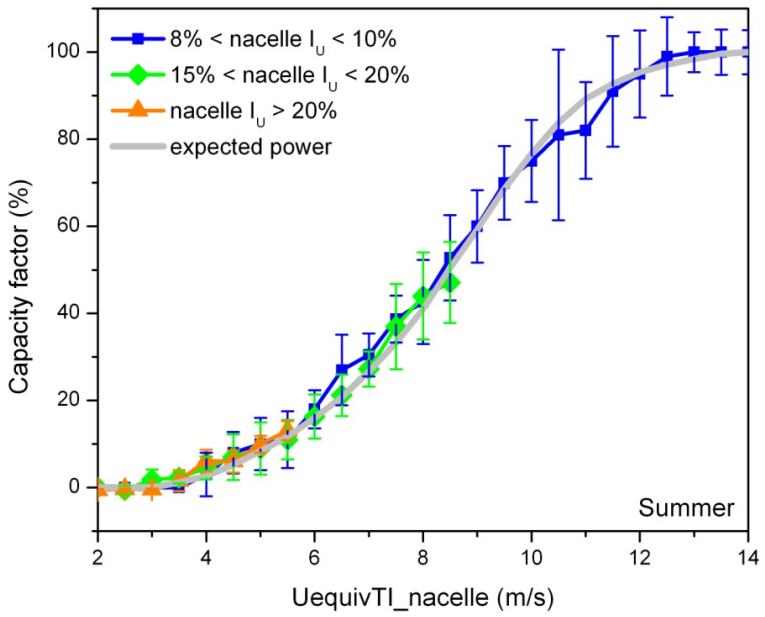

Figure 18: Summer stability-dependent power curves for Turbine #1 based on nacelle cup anemometer I_U. Plotted are the mean capacity factor ± one standard deviation for each 0.5 m s^{-1} wind averaging bin during strongly stable or stable (I_U < 10%), slightly convective (15% < I_U < 20%), and convective (20% < I_U < 30%) conditions, as well as the manufacturer's power curve (expected power).

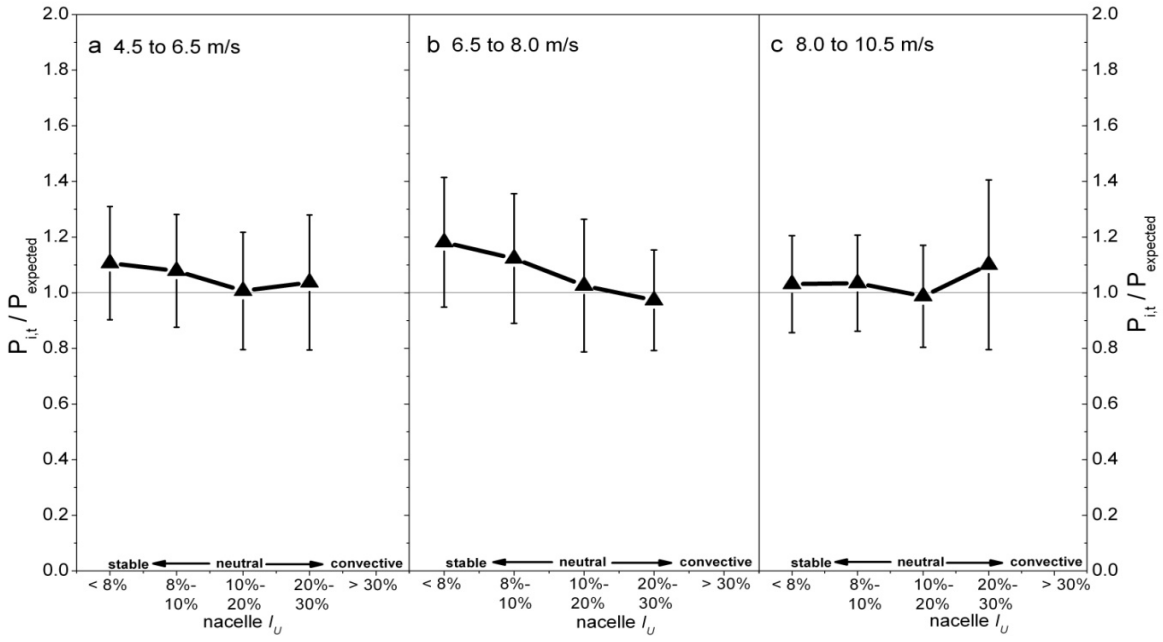

Figure 19: Mean (± one standard deviation) normalized power output versus nacelle I_U-based stability for low (4.5 to 6.5 m s^{-1}), moderate (6.5 to 8.0 m s^{-1}) and high (8.0 to 10.5 m s^{-1}) wind velocity ($U_{equivTI\_nacelle}$) ranges during the spring and summer period for Turbine #1. A normalized power value of 1 indicates that the amount of power generated is equal to the expected power output. There is no strong evidence that turbulence either improves or inhibits power production when nacelle I_U is used to classify stability regimes.

4.6.2 Stability parameter: SODAR α

Based on the work of Rareshide et al. (2009) and others, wind shear across the rotor disk is expected to influence power production. Three stability classes (stable ($\alpha > 0.2$), convective ($0.0 < \alpha < 0.1$) and strongly convective ($\alpha < 0.0$)) are defined based on four wind shear calculations, and the corresponding power curves are plotted in Figure 20. The data from Turbine #1 during the spring and summer months indicate that the wind shear across the top half of the rotor disk (80 m to 120 m AGL) does not significantly impact power output – the lines for the three stability classes are nearly indistinguishable (Fig 20c). In contrast, greater power differences were observed when we used cup anemometer α (Fig 20a) or SODAR α (Fig 20b) at lower heights (40 m or 50 m to 80 m) or throughout the entire rotor (40 m to 120 m) (Fig 20d) to define stability. More power was produced by the turbine when conditions in the lower half or entire rotor indicated stable conditions than during convective or strongly convective conditions. For example, at 8.0 m s^{-1} in Figure 20d, the average capacity factor during strongly convective conditions was 39% ± 7% and during stable conditions was 48% ± 9%, compared to an expected capacity factor of 41%. In the colder months (not shown), the relationship between α and power production was less robust.

These data show that, in spring and summer, higher values of shear in the lower half or entire rotor disk lead to slightly higher energy production compared to periods of low shear. This phenomenon could indicate that even after rotor-averaged wind speed and turbulence are taken into effect, as with Eq (8), high wind shear can positively affect the performance of these particular turbines. Figure 21 also shows that more power is produced during times of high shear, but by normalizing power production, the largest differences between stable and convective conditions is now apparent for the lowest wind speed range (Fig 21a).

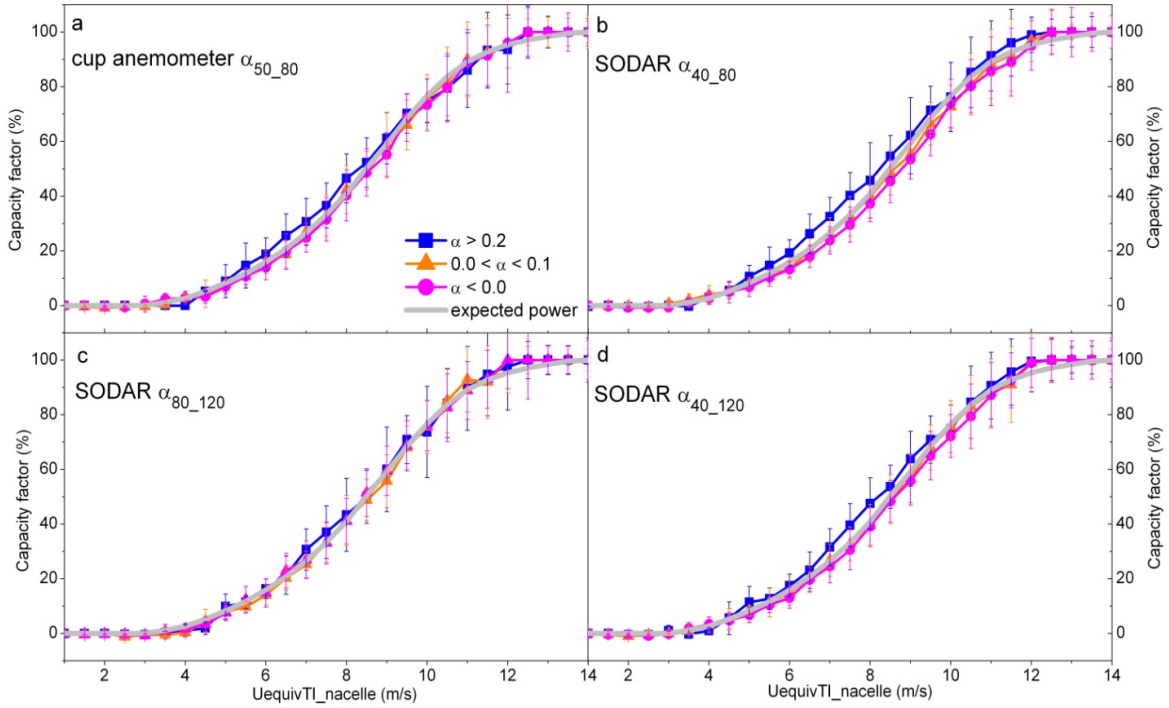

Figure 20: Spring and summer power curves for Turbine #1 during strongly convective ($\alpha < 0.0$), convective ($0.0 < \alpha < 0.1$), and stable or strongly stable ($\alpha > 0.2$) atmospheric conditions. Wind shear is based on (a) meteorological tower wind speed measurements and SODAR measurements of wind speed across (b) the lower half of the rotor, (c) the upper half of the rotor, and (d) across the entire rotor. Plotted are mean capacity factor ± one standard deviation and the expected power curve.

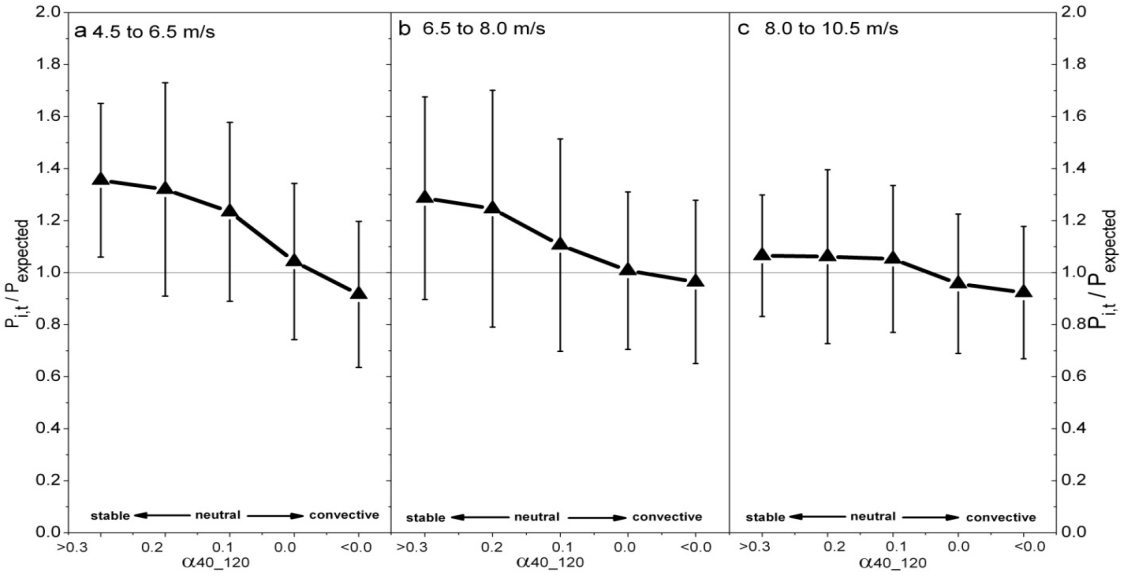

Figure 21: Mean (± one standard deviation) normalized power versus SODAR α-based stability for low (4.5 to 6.5 m s^{-1}), moderate (6.5 to 8.0 m s^{-1}) and high (8.0 to 10.5 m s^{-1}) wind speeds ($U_{equivTI\_nacelle}$) at Turbine #1 shows that more power than expected was produced during very stable and stable conditions than during very convective and convective conditions. The power differences are most acute at low wind speeds.

4.6.3 Stability parameter: SODAR I_U

Other researchers (e.g., Elliot and Cadogan 1990) have found that power curves can show a clear dependence on turbulence intensity, with distinct power curves emerging from data segregated by turbulence intensity I_U. We also observed distinct power curves when the power data were stratified by SODAR-based turbulence intensity (Figs 22-24). The most significant power curve differences occurred between very stable and very convective conditions when wind speed was between 5.5 and 10 m s^{-1}. In general, Turbine #1 over-performed during stable or strongly stable conditions and under-performed during strongly convective conditions for wind speeds above 5 m s^{-1}. For example when the wind was on average 7.5 m s^{-1}, mean capacity factor was 40% ± 6% during strongly stable/stable conditions, 32% ± 8% during convective conditions, and 26% ± 6% during strongly convective conditions, compared to the expected capacity factor of 33%. This stability trend was not unique to Turbine #1. Figure 23 shows power curves stratified by SODAR I_U at each of the six turbines. Underperformance during high turbulence conditions was seen at all of the turbines and the greatest underperformance was observed at Turbine #5. In Figures 22 and 23, the stability effects on power performance are much more apparent than they are in Figure 18 or 19 which use nacelle-based I_U to define the stability regimes.

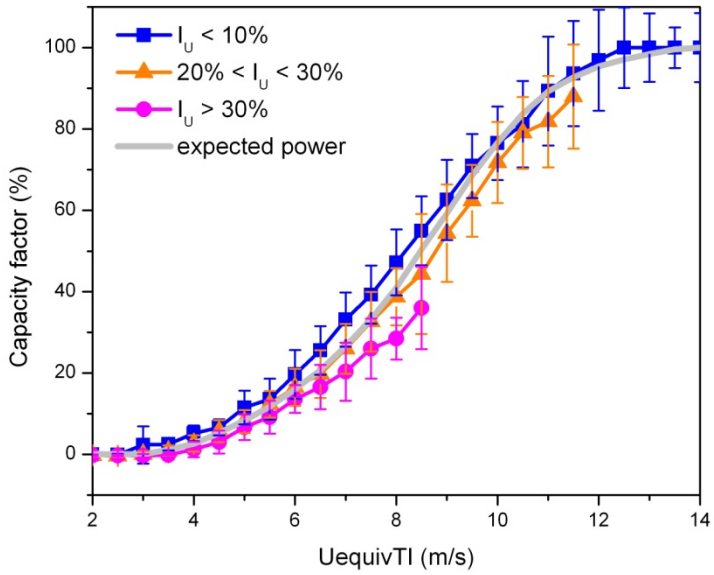

Figure 22: Stability-dependent power curves for Turbine #1 based on SODAR I_U in spring and summer. Plotted are the mean capacity factor ± one standard deviation for each 0.5 m s^{-1} wind averaging bin during strongly stable or stable (I_U < 10%), convective (20% < I_U < 30%), and strongly convective conditions (I_U > 30%). Also plotted is the manufacturer's power curve (expected power).

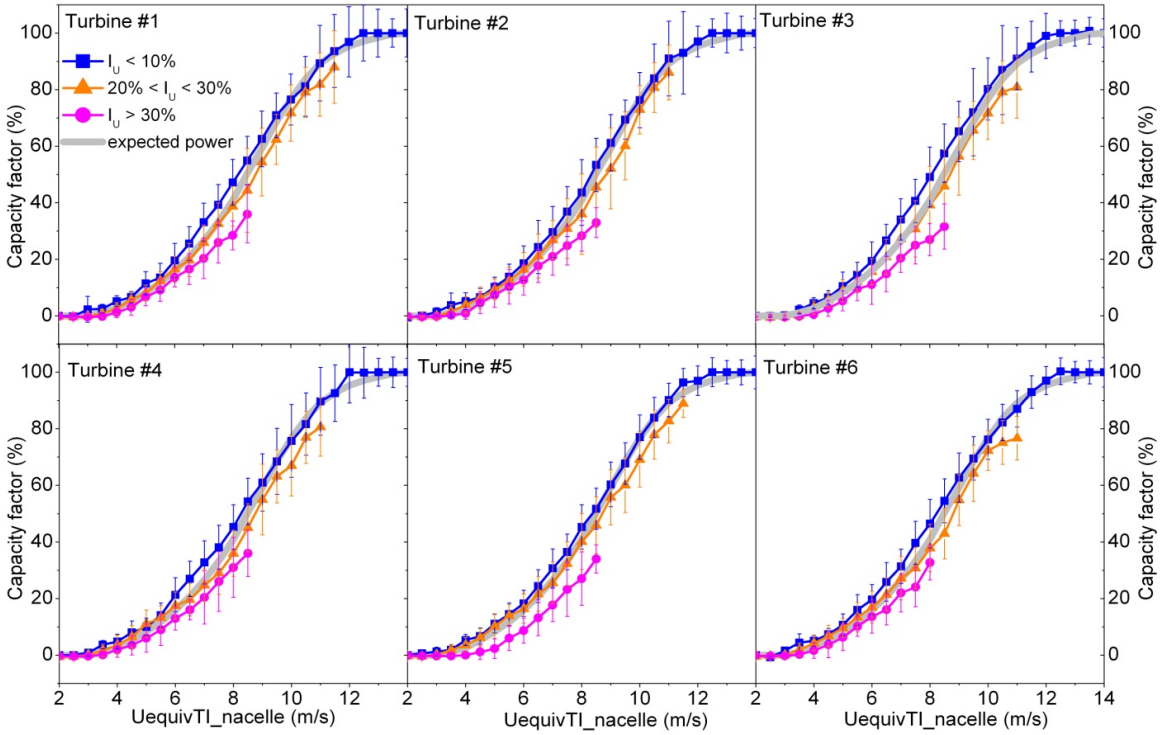

Figure 23: Stability stratified power curves for the six individual turbines, Turbine #1 – Turbine#6 during spring and summer months. Stability is based on hub-height SODAR turbulence intensity. Shown are mean capacity factor ± one standard deviation during strongly stable, convective and strongly convective conditions as well as the expected power curve.

Figure 24 provides a closer examination of how turbulence affects power production during different wind speed ranges for Turbine #1. The differences in power amongst stability regimes are most extreme at low wind speeds. Over-performance was observed at all wind speeds during stable or strongly stable conditions but more so at the lower velocities. When turbulence intensity was moderate to high ($17.5\% < I_U < 30\%$) and the atmosphere was convective, Turbine #1 either over-performed or under-performed depending on the equivalent wind speed. Under-performance during slightly convective or convective conditions was observed at moderate and high wind speeds while over-performance was observed at low wind speeds. During time of very high turbulence, the turbine consistently under-performed regardless of wind speed.

Although direct comparison to previous power curve studies is not possible, because of large values of turbulence intensity observed at this site, it is interesting to note that Elliot and Cadogan (1990) did not find similar patterns of performance. They found over-performance during neutral regimes, with $10\% < I_U < 15\%$, and consistent under-performance for regimes with $I_U < 10\%$ as opposed to the over-performance found here. Some of the difference may be ascribed to different turbine technologies; Elliot and Cadogan's data comes from the two-bladed MOD-2 turbine, and the turbines in the present study are three-bladed. More similar to what we observed during slightly convective conditions at our site, Rareshide et al. (2009) present differences between ($5\% < I_U < 11\%$) and ($11\% < I_U < 17\%$), with an implied over-performance at low wind speeds for the ($11\% < I_U < 17\%$) regime and implied under-performance at high wind speeds for the ($11\% < I_U < 17\%$) regime; turbine height information is not provided for their study.

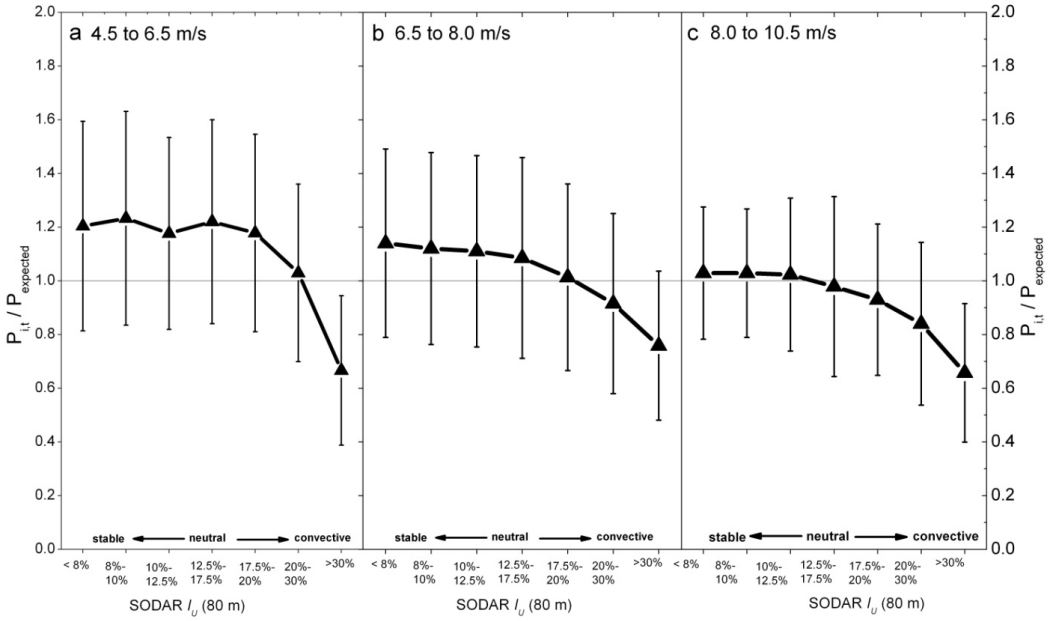

Figure 24: Mean (± one standard deviation) normalized power output versus SODAR I_U-based stability class for low (4.5 to 6.5 m s^{-1}), moderate (6.5 to 8.0 m s^{-1}) and high (8.0 to 10.5 m s^{-1}) wind velocity ($U_{equivTI\_nacelle}$) ranges during the spring and summer period for Turbine #1. A trend is clearly visible: power productivity declines as turbulence intensity increases. The largest stability effects are apparent at low wind speeds.

4.6.4 Stability parameter: *TKE*

In this section, the power curves are stratified by turbulence kinetic energy, which includes the vertical component of turbulence as well as the horizontal turbulence components which were included in turbulence intensity (I_U). This calculation is possible only because of access to the 3-dimensional velocity SODAR data, with which *TKE* was calculated. To our knowledge, this is the first attempt to stratify power data by a complete measure of turbulence (e.g., *TKE*). Figure 25 shows the spring and summer power curves at Turbine #1when *TKE* is used to classify stability. Likewise to the I_U -stratified power curves (Figures 22 and 23), distinct power differences are observed when the power data are stratified by SODAR-based *TKE*. The most significant differences occurred between very stable or stable and very convective

conditions; these differences approach 20%. For example, at 9 m s^{-1}, the average capacity factor was 61% ± 9% during stable conditions, compared to 44% ± 11% during strongly convective conditions. At this wind speed, the expected capacity factor is 60%. Figure 26 provides a closer examination of how turbulence kinetic energy affects power production during different wind speed ranges for Turbine #1. The power differences amongst stability regimes are most evident at low to moderate wind speeds, although wind speed appears to have less of an effect on how *TKE*-based stability impacts power production than was observed for SODAR I_U (Figure 24).

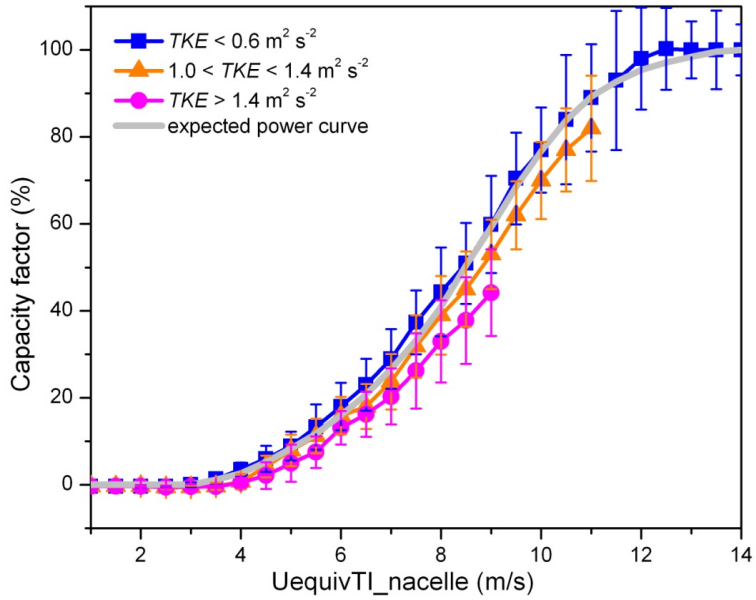

Figure 25. Spring and summer-time stability-dependent power performance curves for Turbine #1 based on SODAR *TKE* at hub-height. Plotted are the mean capacity factor ± one standard deviation for each 0.5 m s^{-1} wind averaging bin during strongly stable or stable (*TKE* < 0.6 m^2 m^{-2}, convective (1.0 m^2 m^{-2} < *TKE* < 1.4 m^2 m^{-2}), and strongly convective conditions (*TKE* > 1.4 m^2 m^{-2}). Also plotted is the manufacturer's power curve (expected power).

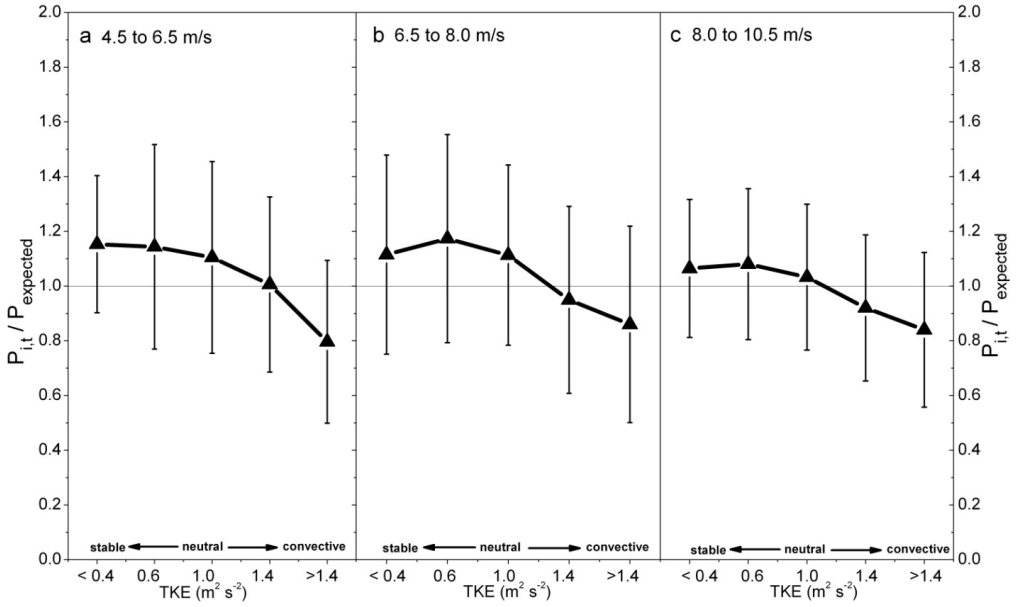

Figure 26: Mean (± one standard deviation) normalized power output versus SODAR *TKE*-based stability class for low (4.5 to 6.5 m s^{-1}), moderate (6.5 to 8.0 m s^{-1}) and high (8.0 to 10.5 m s^{-1}) wind velocity ($U_{equivTI\_nacelle}$) ranges during the spring and summer period for Turbine #1. Wind speed has less of an effect on how stability impacts power production when *TKE* is used to define stability.

4.6.5 Summary of power dependency on stability regime

The results from stratifying the power curves with different stability parameters are summarized in Figure 27 for the 6 to 10 m s^{-1} wind speed range. Very convective conditions led to systematic under-performance of the turbines at this wind farm when the stability parameter was based on SODAR data. The largest declines in power production occurred when stability conditions were based on the amount of turbulence present in the rotor disk, either from using the SODAR I_U or SODAR *TKE* to classify the 10-minute power data. Higher amounts of wind shear in the rotor disk also led to higher power performance. A trend in stability-related power production is clear at this wind farm: decreasing amounts of power are produced as the boundary layer transitions from stable to convective regimes.

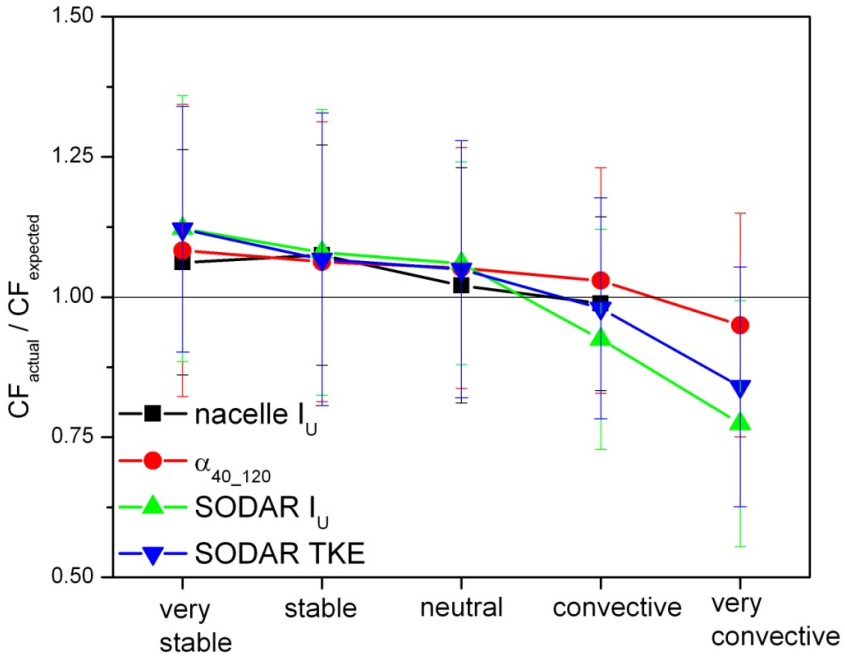

Figure 27: Mean (± one standard deviation) normalized capacity factor for the four stability parameters according to stability regime. This figure includes only time periods when the nacelle-adjusted "true-flux" equivalent wind speed was between 6 and 10 m s^{-1}.

Power performance at this wind farm is also summarized with the power coefficient, C_p , calculated with Eq (10). The turbines are most efficient at converting wind into electricity at moderate wind speeds: 6 to 9 m s^{-1}. Figure 28 shows that stability conditions influence the turbine's power efficiency, especially at this wind speed range. Power coefficients were much lower during convective conditions than during stable conditions when stability was based on either SODAR I_U or *TKE* and less so when stability was based on wind shear. For example at the 6 to 9 m s^{-1} wind speed range, average C_p during stable conditions was 0.43 ± 0.11 and 0.36 ± 0.11 during convective conditions when stability was based on SODAR I_U. In contrast, little to no differences in C_p were observed when stability was based on nacelle I_U.

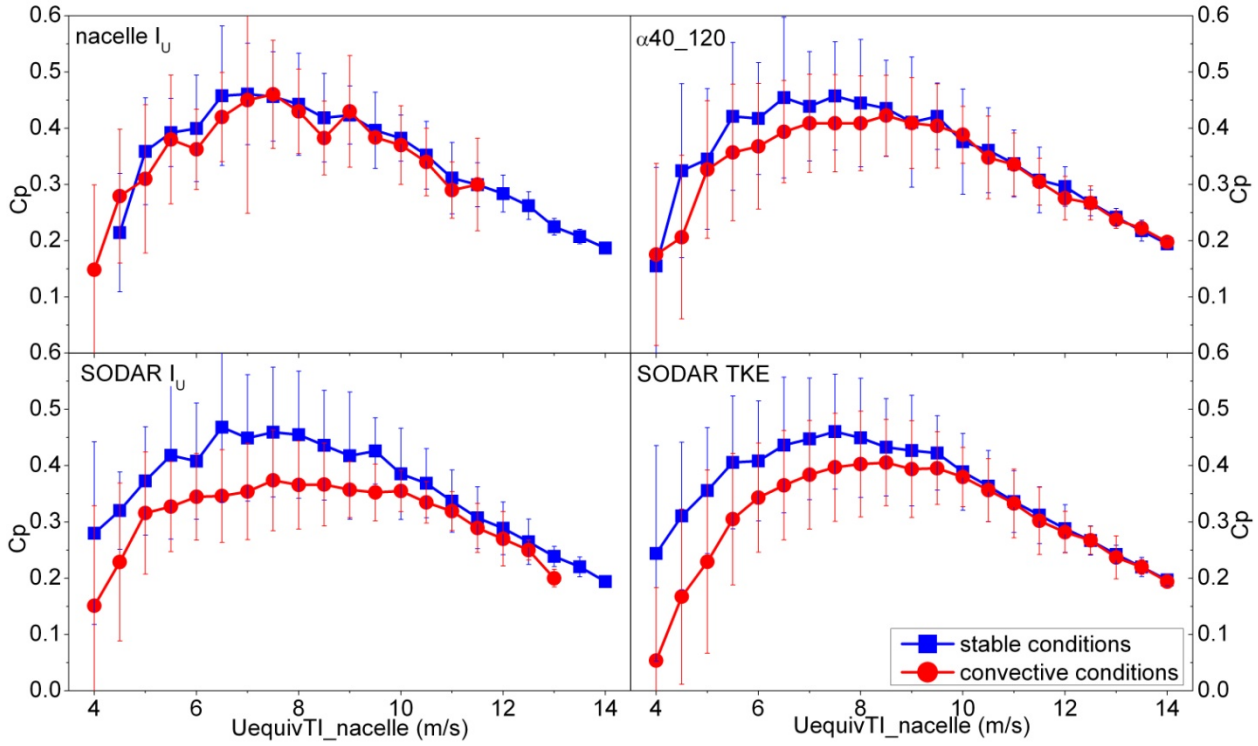

Figure 28: Average (± one standard deviation) power coefficient as a function of wind speed and stability parameter during stable or strongly stable and convective or strongly convective conditions at Turbine #1 during spring and summer months. The largest differences in C_p between stable and convective conditions occur when SODAR I_U or *TKE* is used to classify boundary layer stability.

5. Discussion

With the rapid expansion of wind farms and the significant penetration of wind energy into power markets, accurate estimates of power availability and the dependence of power on atmospheric conditions are required, particularly for the industrial-scale turbines with rotor disks spanning more than 50m. In this study, data from an operating wind farm, in conjunction with a unique meteorological dataset including remote-sensing SODAR, meteorological tower anemometers, and an offsite research-grade surface flux station was explored to quantify the utility of various measures of atmospheric stability as well as document the impact of atmospheric stability on power collection efficiency.

Most wind farms in the contiguous U.S. exhibit peak power production in January and lowest production in August (Lu et al. 2009). In contrast, this wind farm exhibited maximum capacity factors on spring and summer nights. The power season at this location is driven largely by regional climatology which produces a warm, dry season with strong thermal gradients and strong on-shore flow, and a cool, wet season with synoptic storm events. The summer peak in power coincided with higher wind speeds in the rotor swept-area, and in particular, with maximum wind speeds found at the top of the rotor (100 to 120 m AGL) during stable nighttime conditions. In most cases, the power law ($\alpha = 0.14$) did not accurately predict the vertical wind speed profiles observed in the turbine swept area. Considerable deviation from the power law profile has also been observed by Antoniou et al. (2006) and Wagner et al. (2009). In our study, a constant wind shear value of 0.14 underestimated the true wind velocity at the top of the rotor during stable conditions by up to 2 m s^{-1}, while during convective conditions, the power law overestimated wind speed by an equal amount.

Because of this variability in wind shear, the hub-height wind speed measurement did not accurately represent the average wind speed over the rotor swept-area except during neutral conditions. This observation has been made others including Elliott and Cadogan (1990), Frandsen et al. (2000), and Wagner et al. (2009). Early work by Elliott and Cadogan (1990) suggested that a significant source of error in power curves is created by the differences between the true disk-averaged velocity and hub-height velocity. We also found this to be true: the difference between "true-flux" equivalent wind speed and hub-height wind speed was most acute during stable conditions at our wind farm and maximum error between the two was on the order of 1.5 to 2 m s^{-1}. Power curves in our study therefore relied on the "true-flux" equivalent wind speed, which accounts for winds across the rotor disk as well as turbulence intensity for the power curves, and builds on the theory and development of equivalent wind speed found in Wagner et al. (2009).

A high degree of turbulence intensity was observed with the SODAR located at this wind farm; maximum I_U values exceed those values published in the literature. This disparity can be attributed to several factors, including a location in mildly complex terrain: other studies have either been in the relatively flat Midwest (USA) (Rareshide et al. 2009), flat Denmark (Wagner et al. 2009), or flat pastureland in England (Sumner and Masson 2006). Our hub-height turbulence intensities ranged from less than 8% to over 30% and were highest during convective conditions and lowest during stable conditions. During stable conditions, turbulence intensity decreased with height and increased sharply with height during convective conditions. These profiles agree with other studies (e.g., Pichugina et al. 2008, Wagner et al. 2009), which observe that wind conditions tend to differ above and below the turbine hub.

The on-site wind shear, SODAR-based I_U and *TKE* compared well with the more physically-based Obuhkov length. In contrast, the nacelle-based I_U, which is available at most wind farms, was in high disagreement with the other stability parameters and greatly underestimated the frequency of convective conditions. Other studies have determined stability based on one or two of these parameters (e.g., Motta and Barthelmie 2005, van den Berg 2008) but ours is the first study of our knowledge to compare such a large set of independent stability parameters. Measurements of turbulence kinetic energy were available at this wind farm only because of the presence of the SODAR, although deployment of 3-D sonic anemometers on meteorological towers could enable quantification of *TKE*.

Once the stability parameters were checked for accuracy against the Obukhov length, our wind farm data were segregated into five classes: strongly stable, stable, neutral, convective, and strongly convective. In both spring and summer, average capacity factors and power coefficients exhibited a negative relationship with SODAR turbulence intensity and turbulence kinetic energy, and positive relationship with wind shear across the entire rotor disk. Large amounts of turbulence at hub-height inhibited power production while high wind shear across the rotor disk increased turbine power output. High wind shear increased power production because during these periods the equivalent wind speed was greater than the hub-height wind speed owing to faster winds in the upper portion of the rotor. More power produced during times of high wind shear has likewise been observed by Antoniou et al. (2009b) for multi-MW tall turbines in moderately complex terrain. In contrast to wind shear and SODAR-based turbulence, a relationship between power production and nacelle-based turbulence intensity was not found at our site, probably because of the poor ability of nacelle I_U to predict boundary layer stability. Power production was also not related to stability during the winter or autumn periods regardless

of the parameter chosen to define stability. In the winter and autumn months, the stable and convective vertical wind speed profiles are much more alike than are observed during spring and summer periods.

After normalizing the actual power output by the expected power amount, it became apparent that the relationship between turbulence (either horizontal turbulence intensity or turbulence kinetic energy) and power production was strongest at lower wind speeds although this is not clearly visible in the power curves because of low capacity factors found in this wind speed range. The largest stability effects on power production were visible when power was normalized and the "true flux" equivalent wind speed was less than 6.5 m s^{-1}. A weakening of stability effects on power production at very high winds speeds may be attributable to the fact that as wind speed increases, the atmospheric stability regime approaches neutral because thermal gradients dissipate as wind shear increases. During neutral conditions, power production at this wind farm varied little from the expected values.

Other studies have looked at the influence of wind speed on stability-power curves but the results are not in universal agreement. Hunter et al. (2001) found that at moderate wind speeds (~ 5.5 m s^{-1}), more power was generated under high wind shear conditions than during times of little or no wind shear. For wind speeds above 8.5 m s^{-1}, they observed the opposite effect: wind shear negatively impacted power production. In comparison, we found that for every wind speed, wind shear values above 0.2 had a positive effect on power production while negative wind shear always had a negative impact on power, although lower wind speeds did appear to amplify the effects of wind shear on stability. In a similar manner, we found that high amounts of turbulence (either indicated by turbulence intensity or turbulence kinetic energy), decreased power production, especially at lower wind speeds. This is in contrast with

observations made by Elliott and Cadogan (1990), whereby they found that higher turbulent conditions led to more power being produced. It is important to note the differences between our study and theirs. Elliott and Cadogan (1990) looked at two-bladed turbines and found that the rotor-averaged wind speed was less than the hub-height wind speed under stable conditions. Therefore, during stable conditions, less energy was available to the turbine than during convective conditions. In contrast, our study used modern 3-bladed turbines and we found that the rotor-averaged wind speed was greater than the hub-height wind speed under stable conditions. Thus, more energy was available to the turbines in our study during stable conditions than during convective conditions. We observed a negative impact of turbulence on power production: the amount of power decreases as the boundary layer becomes more convective, coinciding with lower "true-flux" equivalent wind speeds, higher turbulence and lower wind shear throughout the rotor disk than during stable conditions.

Lastly, our stability stratified power curves show the importance of having sophisticated meteorological measurements instead of relying on cup anemometers for hub-height wind speed and direction. We found large, fundamental differences between SODAR and cup anemometer measured turbulence intensity and wind speed. Fundamentally, these two instruments work very differently. The SODAR measures vectors over a volume average while the cup anemometer does scalar averaging on a point measurement. Vector averaging can be up to 5% lower than scalar averaging although the mean difference is around 2 to 3% (Moore and Bailey 2009). Our SODAR velocity standard deviations were larger than the ones obtained with a cup anemometer. Wagner et al. (2008) also observed this phenomenon in their power curve study and attributed the difference to the fact that SODAR measurements are very noisy and the profiles are often distorted. Precipitation can induce acoustic noise and accounted for our lower data recovery

during the autumn and winter periods. In order to remove this source of error in the SODAR data, our study reported findings from the relatively dry spring and summer months. Cup anemometers have been documented to overestimate the true mean wind velocity (Hölling et al. 2007), more so when turbulence intensity is high or wind velocity is low because of non-linearity effects (Finnigan 2002). A recent study by Kline (2008) showed that cup anemometers overestimate the true wind velocity by 0.0975% per 1% horizontal turbulence intensity. Therefore, if the horizontal turbulence intensity is 15% and the actual mean wind speed is 8.0 m s^{-1}, the cup anemometers could measure a wind velocity closer to 8.2 m s^{-1}. As turbine power is related to the wind velocity cubed, this error would result in an overestimation of 2.6% from the amount of power actually produced. At very high turbulence intensities (I_U > 40%), such as those periodically observed at this wind farm, Yahaya and Frangi (2003) found that the relative difference between the mean wind velocities measured by a co-located sonic anemometer and cup anemometer was even higher and approached 6%. Furthermore, cup anemometers are not suitable for making turbulence measurements because they respond faster to increases in velocity than to decreases which leads to errors in the turbulence intensity measurement (Weber 1998 and Yahaya and Frangi (2003).

6. Conclusions

The main conclusions that can be drawn from the analysis are:

(1) Boundary layer stability can be quantified accurately at wind farms in mildly complex terrain by measuring wind shear, either with a tall tower or SODAR, at multiple heights in the rotor disk or by measuring turbulence at hub-height with SODAR.

(2) More accurate power curves are produced when power is plotted as a function of "true-flux" equivalent wind speed instead of hub-height wind speed. This suggests that both wind shear and turbulence are important factors in power production at this tall turbine site.

(3) Turbulence-based stability parameters, either turbulence intensity or turbulence kinetic energy, best explained why a turbine produced more or less power than expected. For a given wind speed, less power is produced by turbines during convective conditions than during stable conditions. The relative power differences are most acute when wind speed is low to moderate.

Our work shows promise for using remote-sensing instrumentation to observe complete profiles of wind speed, wind direction and turbulence across a nearly 80 m diameter rotor in mildly complex terrain. Our study also shows evidence that turbulence and wind shear play a role in power production, and high-resolution instruments such as SODAR are needed to quantify these parameters across the rotor diameter. The presence of a stable boundary layer in the spring and summer at this wind farm has the same effect on power performance as increasing the wind velocity at hub-height by 0.5 to 1 m s^{-1}. The opposite is true for strongly convective conditions: very high amounts of turbulence have the same effect on power performance as decreasing the wind velocity at hub-height by 0.5 to 1 m s^{-1}. Finally, because of this significant impact of stability on turbine performance, approaches to forecasting wind energy performance should be well-grounded in meteorological approaches that can successfully forecast atmospheric stability in the lower boundary layer. This goal can be quite challenging in regions of complex terrain. Without correct forecasts of stability, errors in predictions of turbulent mixing or wind shear would likely undermine the performance of a wind energy forecasting model.

7. References

Antoniou I, Jørgensen HE, Mikkelsen T, Frandsen S, Barthelmie R, Perstrup C, Hurtig M. Offshore wind profile measurements from remote sensing instruments. *In*: Scientific proceedings. European Wind Energy Conference and Exhibition, Athens (Greece), 2006.

Antoniou I, Wagner R, Pedersen SM, Paulsen U, Madsen HA, Jørgensen HE, Thomsen K, Enevoldsen P, Thesbjerg L. Influence of wind characteristics on turbine performance. *In*: Scientific proceedings. European Wind Energy Conference and Exhibition, Milan, (Italy), 2007.

Antoniou I, Pedersen SM, Enevoldsen, PB, Lind SO. Uncertainty in power curve measurements caused by wind shear. *In*: Scientific proceedings. American Wind Energy Association, Wind Resource and Project Energy Assessment Workshop, Minneapolis, MN (USA), 2009a.

Antoniou I, Pedersen SM, Enevoldsen PD. Wind shear and uncertainties in power curve measurement and wind resources. *Wind Engineer.* 2009b; 33: 449-468.

AWEA (American Wind Energy Association) Windpower Outlook 2009. Downloaded from http://www.awea.org/pubs/documents/Outlook_2009.pdf on 2 December 2009.

Banta RM. Stable-boundary-layer regimes from the perspective of the low-level jet. *Act Geophys.* 2008; 56: 58-87.

Betz A. *Introduction to the theory of flow mechanics*. Pergamon Press, Oxford, England, 1966, 281 p.

Blackadar AK. Boundary layer wind maxima and their significance for the growth of nocturnal inversions. *Bull. Am. Meteorol. Soc.* 1957; 38: 283-290.

Christensen CJ, Dragt JB (eds). *Accuracy of power-curve measurements*. Risø-M-2632. Risø National Laboratory, Roskilde, Denmark, 1986.

Cosack N, Emeis S, Kuhn M. On the influence of low-level jets on energy production and loading of wind turbines. *In*: *Wind Energy*, Proceeding of the Euromech Colloquium, Eds. Peinke J, Schaumann P, Barth S., Springer Berlin Heidelberg, New York, 2007; 325-328 pp.

Coulter RL, Kallistratova MA. The role of acoustic sounding in a high-technology era. *Meteor. Atmos. Phys.* 1999; 71: 3-13.

Crescenti GH. A look back on two decades of Doppler sodar comparison studies. *Bull. Am. Meteorol. Soc.* 1997; 78: 651-673.

de Vries O. *Fluid dynamic aspects of wind energy conversion*. AGARD-AG-243, 1978.

Elliott DL, Cadogan JB. Effects of wind shear and turbulence on wind turbine power curves. *In*: Scientific proceedings. European Community Wind Energy Conference and Exhibition, Madrid (Spain), 1990.

Elliott DL, Holliday C, Barchet W, Foote H, Sandusky W. *Wind Energy Resource Atlas of the United States*. DOE/CH 10093-4, Golden, Colorado: Solar Energy Research Institute, 1987, 210 pp.

Emeis S, Harris M, Banta RM. Boundary-layer anemometry by optical remote sensing for wind energy applications. *Meteor. Zeitschr*. 2007; 16: 337-347.

Enercon. Construction of world's most powerful wind turbines in progress in Emden, 9/28/2007. Downloaded from http://www.enercon.de/www/en/nachrichten.nsf/41657424de23a0b8c1256ed10041a39f/6230d2639aa384d9c125736e004679c2?OpenDocument on 2 December 2009.

Fransden S. On uncertainties in power performance measurements. *In:* Scientific Proceedings. 6th ASME Wind Energy Symposium, American Society of Mechanical Engineers, New York, 1987.

Fransden S, Antoniou I, Hansen JC, Kristensen L, Madsen HA, Chaviaropoulos B, Douvikas D, Dahlberg JA, Derrick A, Dunbabin P, Hunter R, Ruffle R, Kanellopoulos D, Kapsalis G. Redefinition power curve for more accurate performance assessment of wind farms. *Wind Energy* 2000; 3: 81-111.

Gottschall J, Peinke J. How to improve the estimation of power curves for wind turbines. *Environ. Res. Lett.* 2008; 3: 1-7.

Hand, MM, Kelley ND, Balas MJ. *Identification of wind turbine response to turbulent inflow structures.* NREL/CP-500-33465, 2003.

Hölling M, Schulte B, Barth S, Peinke J. Sphere anemometer – a faster alternative solution to cup anemometry. The Science of Making Torque from Wind. *J Phys*: Conference Series 75, 2007: 012064.

Honhoff S. Power Curves – The effect of environmental conditions. *In*: Scientific proceedings. GE Wind, AWEA Wind Speed and Energy Workshop, Portland, OR (USA), 2007.

Hunter R, Pedersen TF, Dunbabin P, Antoniou A, Frandsen S, Klug H, Albers A, Lee WK. *European wind turbines testing procedure developments*. *Task 1: Measurement method to verify wind turbine performance characteristics.* Risø National Laboratory, Roskilde, RISOE R-1209(EN), 2001.

International Electromechanical Commission (IEC). *Wind turbine generator systems part 121: power performance measurements of grid connected wind turbines*. Draft Technical Report No, IEC 61400-121, 2003.

Kaimal JC, Finnigan JJ. *Atmospheric boundary layer flows – their structure and measurement*. Oxford University Press: New York, 1994.

Kaiser K, Hohlen H, Langreder W. Turbulence correction for power curves. *In*: Scientific proceedings. European Wind Energy Conference and Exhibition, Madrid (Spain), 2003.

Kelley ND, Osgood RM, Bialasiewisz JT, Jakubowski A. Using wavelet analysis to assess turbulence/rotor interactions. *Wind Energy* 2001; 3: 121-134.

Kelley ND, Shirazi M, Jager D, Wilde S, Adams J, Buhl M, Sullivan P, Patton E. *Lamar low-level jet project interim report.* NREL/TP-500-34593. Golden, CO, National Renewable Laboratory, 2004.

Kline J. Addressing bias in wind measurements: Part 1. *In*: Scientific proceedings. AWEA Wind Resource and Project Energy Assessment Workshop, Portland, Oregon (USA), 2008.

Langreder W, Højstrup J, Kaiser K, Hohlen H. Turbulence correction for power curves. *In*: Scientific proceedings. European Wind Energy Conference and Exhibition, London (GB), 2004.

Larsen SE, Gryning SE, Jensen NO, Jorgensen HE, Mann J. Mean wind and turbulence in the atmospheric boundary layer above the surface layer. *In*: *Wind Energy*, Proceedings of the Euromech Colloquium, Eds. Peinke J, Schaumann P, Barth S., Springer Berlin Heidelberg, New York, 2007; 21-25 pp.

Lu X, McElroy MB, Kiviluoma J. Global potential for wind-generated electricity. *Proc. Nat. Acad. Sci.* 2009; 106:10933-10938.

Lundquist JK. Intermittent and elliptical inertial oscillations in the atmospheric boundary layer. *J Atmos. Sci.* 2003; 60: 2661-2673.

Lundquist JK, Mirocha JD. Interaction of nocturnal low-level jets with urban geometries as seen in Joint Urban 2003 data. *J Appl. Meteorol. Clim.* 2008; 47: 44-58.

Mahrt L, Sun J, Blumen W, Delany T, Oncley S. Nocturnal boundary-layer regimes. *Boundary-layer Meteorol.* 1998; 88: 255-278.

Mahrt L. Stratified atmospheric boundary layers. *Boundary-layer Meteorol.*1999; 90: 375-396.

Mahrt L, Vickers D, Nakamura R, Soler MR, Sun J, Burns S, Lenschow DH. Shallow drainage flows. *Boundary-layer Meteorol.* 2001; 101: 243-260.

Mahrt L, Vickers D. Contrasting vertical structures of nocturnal boundary layers. *Boundary-layer Meteorol*. 2002; 105: 351-363.

Magnusson M, Smedman A.-S. Air flow behind wind turbines. *J. Wind Eng. Ind. Aerodyn.* 1999, 80: 169-189.

Monin AS, Obukhov AM. Basic laws of turbulent mixing in the ground layer of the atmosphere. *Trans. Geophys. Inst.* 1954; 151: 163-187.

Moore KE, Bailey BH. Recommended practices for the use of SODAR in wind energy resource assessment, Integrated Environmental Data, LLC, 2009, 13 pp.

Motta M, Marthelmie RJ, Vølund P. The influence of non-logarithmic wind speed profiles on potential power output at Danish offshore sites. *Wind Energy* 2005; 8: 219-236.

Nieuwstadt FTM. The turbulent structure of the stable, nocturnal boundary layer. *J Atmos. Sci.* 1984; 41: 2202-2216.

Obukhov AM. Turbulence in an atmosphere with a non-uniform temperature. *Bound.-layer Meteor.* 1971; 2: 7-29.

Panofsky HA, Dutton JA. *Atmospheric turbulence: models and methods for engineering applications.* John Wiley and Sons, New York (US), 1984, 397 pp.

Pichugina YL, Banta RM, Kelley ND, Brewer WA, Sandberg SP, Machol JL, Jonkman BJ. Remote sensing of the nocturnal boundary layer for wind energy applications. 14th Internat. Sympos. for the Advancement of Boundary Layer Remote Sensing, IOP Conf. Series: Earth and Environmental Science 2008; 1: doi:10.1088/1755-1307/1/1/012048.

Piper M, Lundquist JK. Surface layer turbulence measurements during a frontal passage. *J Atmos. Sci.* 2004; 61, 1768-1780.

Rareshide E, Tindal A, Johnson C, Graves AM, Simpson E, Bleeg J, Harris T, Schoborg D. Effects of complex wind regimes on turbine performance. *In*: Scientific proceedings. American Wind Energy Association WINDPOWER Conference, Chicago, Ill (USA), 2009.

Rohatgi, J. An analysis of the influence of atmospheric stability on vertical wind profiles – its influence on wind energy and wind turbines. *Wind Engineering* 1996; 20: 319-332.

Rohatgi J, Barbezier G. Wind turbulence and atmospheric stability – their effects on wind turbine output. *Renewable Energy* 1999; 16: 908-911.

Sathe A, Bierbooms W. Influence of different wind profiles due to varying atmospheric stability on the fatigue life of wind turbines. *J Phys Conference Series* 2007; 75: 1-7.

Storm B, Dudhia J, Basu S, Swift A, Giammanco I. Evaluation of the weather research and forecasting model on forecasting low-level jets: implications for wind energy. *Wind Energy* 2009; 12: 81-90.

Stull RB. *An introduction to boundary layer meteorology*. Kluwer Academic Publishers, Dordrecht, The Netherlands, 1988, 670 pp.

Sumner J, Masson C. Influence of atmospheric stability on wind turbine power performance curves. *J. Sol. Energy Eng.* 2006; 128: 531-537.

Tindal A, Johnson C, LeBlanc M, Harman, K, Rareshide, E, Graves A-M. Site-specific adjustments to wind turbine power curves. *In*: Scientific proceedings. American Wind Energy Association WINDPOWER Conference, Houston, Texas (USA), 2008, 11p.

van den Berg GP. Wind turbine power and sound in relation to atmospheric stability. *Wind Energy* 2008; 11: 151-169.

van Wijk AJM, Beljaars ACM, Holtslag AAM, and Turkenburg WC. Evaluation of stability corrections in wind speed profiles over the North Sea. *J. Wind Eng. Ind. Aerodyn*. 1990; 33: 551-566.

Wagner R, Antoniou I, Pedersen SM, Courtney MS, Jørgensen HE. The influence of the wind speed profile on wind turbine performance measurements. *Wind Energy* 2009; 12, 348-362.

Walter K, Weiss CC, Swift A, Chapman J, Kelley ND. Speed and direction shear in the stable nocturnal boundary layer. *J. Sol. Energy Eng.* 2009; 131, 11013 1-7.

Weber RO. Estimators for the standard deviations of the lateral, longitudinal and vertical wind components. *Atmos. Environ.* 1998; 32: 3639-2646.

Wiser R, Bolinger M. *Annual report on U.S. wind power installation, cost and performance trends: 2007.* U.S. DOE Publication DOE/GO-102008-2590. 2009.

Yahaya S, Frangi JP. *Spectral response of cup anemometers*. Laboratoire Environmmement et Developpement Report, Universite Paris, 2003, 3 p.

List of Tables

Table 1. 13
List of the available meteorological instrumentation, variables measured, and measurement heights.

Table 2. 20
Stability classifications for the four stability parameters (Obukhov length, wind shear, turbulence intensity, and turbulence kinetic energy), general atmospheric conditions, and frequency of occurrence during the data period.

List of Figures

Figure 1. 24
Frequency distribution of 10-minute SODAR hub-height, SODAR "true-flux" equivalent, nacelle hub-height, and nacelle-adjusted "true-flux" equivalent wind speed for Turbine #1 during the spring and summer months.

Figure 2. 27
Monthly mean night and day wind speeds at 40 m, 80 m and 120 m heights from SODAR and the meteorological towers show strong seasonality.

Figure 3. 27
Seasonal diurnal plots of 40 m, 80 m, and 120 m mean wind speed show a strong diurnal signal during spring and summer.

Figure 4. 28
Frequency plots of nighttime/daytime wind direction for 40 m, 80 m and 120 m wind velocities during the spring show that winds are predominantly from the WSW at this wind farm.

Figure 5. 29
Percentage of summer time periods classified as stable, neutral or convective according to the four stability parameters: (a) normalized Obukhov length, (b) SODAR wind shear, (c) SODAR turbulence intensity, (d) nacelle turbulence intensity, and (e) SODAR turbulence kinetic energy.

Figure 6. 30
Histogram of 10-minute SODAR wind shear (α_{40_120}) data according to $\frac{z}{L}$ stability class.

Figure 7. 31
Histogram of 10-minute hub-height, SODAR turbulence intensity (I_U) data according to $\frac{z}{L}$ stability class.

Figure 8. 31
Histogram of 10-minute hub-height, SODAR turbulence kinetic energy (*TKE*) data according to $\frac{z}{L}$ stability class.

Figure 9. 32
Diurnal plot of mean wind shear (α) between heights of 40-120 m, 80-120 m, 40-80 m, and 50-80 m AGL by season.

Figure 10. 34
Diurnal plot of mean horizontal turbulence intensity at 40 m, 80 m and 120 m by season. The 80m I_U is based on three instrument locations: SODAR, meteorological tower, and the nacelle.

Figure 11. 35
Meteorological tower-based I_U (80 m) (left panel) and nacelle-based I_U (80 m) (right panel) versus SODAR-based I_U (80 m) for five days during the summer period (Aug. 1- 5) shows a strong bias towards larger SODAR turbulence intensity values.

Figure 12. 36
Wind speed across the rotor diameter (40, 80 and 120 m) according to I_U -defined stability class and month. Also plotted is annual mean wind speed at each height.

Figure 13. 38
Spring vertical profiles (30 m to 150 m) of SODAR mean wind speed (a) and turbulence kinetic energy (b) during very stable (I_U < 8%), stable (8% < I_U < 10%), slightly stable (10% < I_U < 12.5%), neutral (12.5 % < I_U < 15%), slightly convective (15% < I_U < 20%), and convective (I_U > 20%) conditions.

Figure 14. 39
Summer vertical profiles (30 m to 150 m) of SODAR mean wind speed (a) and turbulence kinetic energy (b) during very stable (I_U < 8%), stable (8% < I_U < 10%), slightly stable (10% < I_U < 12.5%), neutral (12.5% < I_U < 15%), slightly convective (15% < I_U < 20%), and convective (I_U >20%) conditions.

Figure 15. 41
Seasonal mean (± one standard deviation) capacity factor and nacelle wind speed for a single turbine, Turbine #1. Wind speeds during the spring and summer were on average 3 m s^{-1} higher than during the cooler months, while the capacity factors were on average 30-36% greater.

Figure 16. 41
Mean diurnal capacity factor at Turbine #1 by season shows large power differences at night between spring/summer periods and winter/autumn periods which approach 50%. Smaller power differences are also observed during the daytime hours.

Figure 17. 43
10-minute power (shown as capacity factor) and wind speed data from a single typical summer day show the best fit between $U_{equivTI\_nacelle}$ and power. Wind speeds plotted are (a) SODAR hub-height wind speed, (b) SODAR "true-flux" equivalent wind speed, (c) nacelle hub-height wind speed, and (d) nacelle-adjusted "true-flux" equivalent wind speed (d).

Figure 18. 46
Summer stability-dependent power curves for Turbine #1 based on nacelle cup anemometer I_U. Plotted are the mean capacity factor ± one standard deviation for each 0.5 m s^{-1} wind averaging bin during strongly stable or stable (I_U < 10%), slightly convective (15% < I_U < 20%), and convective (20% < I_U < 30%) conditions, as well as the manufacturer's power curve (expected power).

Figure 19. 46
Mean (± one standard deviation) normalized power output versus nacelle I_U -based stability for low (4.5 to 6.5 m s^{-1}), moderate (6.5 to 8.0 m s^{-1}) and high (8.0 to 10.5 m s^{-1}) wind velocity ($U_{equivTI\_nacelle}$) ranges during the spring and summer period for Turbine #1.

Figure 20. 48
Spring and summer power curves for Turbine #1 during strongly convective (α < 0.0), convective (0.0 < α < 0.1), and stable or strongly stable (α > 0.2) atmospheric conditions. Wind shear is based on (a) meteorological tower wind speed measurements and SODAR measurements of wind speed across (b) the lower half of the rotor, (c) the upper half of the rotor, and (d) across the entire rotor.

Figure 21. 48
Mean (± one standard deviation) normalized power versus SODAR α-based stability for low (4.5 to 6.5 m s^{-1}), moderate (6.5 to 8.0 m s^{-1}) and high (8.0 to 10.5 m s^{-1}) wind speeds ($U_{equivTI\_nacelle}$) at Turbine #1 shows that more power than expected was produced during very stable and stable conditions than during very convective and convective conditions.

Figure 22. 50
Stability-dependent power curves for Turbine #1 based on SODAR I_U in spring and summer. Plotted are the mean capacity factor ± one standard deviation for each 0.5 m s^{-1} wind averaging bin during strongly stable or stable (I_U < 10%), convective (20% < I_U < 30%), and strongly convective conditions (I_U > 30%).

Figure 23. 50
Stability stratified power curves for the six individual turbines, Turbine #1 – Turbine#6 during spring and summer months. Stability is based on hub-height SODAR turbulence intensity.

Figure 24. 52
Mean (± one standard deviation) normalized power output versus SODAR I_U-based stability class for low (4.5 to 6.5 m s^{-1}), moderate (6.5 to 8.0 m s^{-1}) and high (8.0 to 10.5 m s^{-1}) wind velocity ($U_{equivTI\_nacelle}$) ranges during the spring and summer period for Turbine #1. A trend is clearly visible: power productivity declines as turbulence intensity increases. The largest stability effects are apparent at low wind speeds.

Figure 25. 53
Spring and summer-time stability-dependent power performance curves for Turbine #1 based on SODAR *TKE* at hub-height. Plotted are the mean capacity factor ± one standard deviation for each 0.5 m s^{-1} wind averaging bin during strongly stable or stable (*TKE* < 0.6 m^2 m^{-2}, convective (1.0 m^2 m^{-2} < *TKE* < 1.4 m^2 m^{-2}), and strongly convective conditions (*TKE* > 1.4 m^2 m^{-2}).

Figure 26. 54
Mean (± one standard deviation) normalized power output versus SODAR *TKE*-based stability class for low (4.5 to 6.5 m s^{-1}), moderate (6.5 to 8.0 m s^{-1}) and high (8.0 to 10.5 m s^{-1}) wind velocity ($U_{equivTI\_nacelle}$) ranges during the spring and summer period for Turbine #1.

Figure 27. 55
Mean (± one standard deviation) normalized capacity factor for the four stability parameters according to stability regime. This figure includes only time periods when the nacelle-adjusted "true-flux" equivalent wind speed was between 6 and 10 m s^{-1}.

Figure 28. 56
Average (± one standard deviation) power coefficient as a function of wind speed and stability parameter during stable or strongly stable and convective or strongly convective conditions at Turbine #1 during spring and summer months. The largest differences in Cp between stable and convective conditions occur when SODAR I_U or *TKE* is used to classify boundary layer stability.

Acknowledgements

This work performed under the auspices of the U.S. Department of Energy by Lawrence Livermore National Laboratory under Contract DE-AC52-07NA27344.